UNIVERSITEIT VAN PRETORIA
UNIVERSITY OF PRETORIA
YUNIBESITHI YA PRETORIA

Real-time Non-linear Vehicle Preview Model

by

Bernard Villiers Linström

Submitted in partial fulfilment of the requirements for the degree

Master of Engineering

(Mechanical Engineering)

in the Faculty of

Engineering, Built Environment and Information Technology (EBIT)

at the

University of Pretoria,

Pretoria

February 2015

ERRATA

Throughout this thesis suspension friction is named as the main culprit causing inaccurate roll rate predictions when in actual fact this is caused by an error in the developed vehicle preview model. This error does not have a major effect on the other predicted vehicle states, but only to the roll rate.

Theunis Botha found that the value used to define the distance between the centre of gravity and the roll height of the vehicle was too big. Similarly to the arm of a watch, all points on the arm rotate by the same angle although the points further from the point of rotation have a higher rotational velocity. This explains why the roll angle predictions were accurate, but with inaccurate roll rate predictions.

Due to limited resources this error was not be corrected in this thesis, but was corrected for the paper submitted for publication.

SUMMARY

Title:	Real-time Non-Linear Vehicle Preview Model
Author:	Bernard Villiers Linström
Study Leader:	Prof. P. Schalk Els
Department:	Mechanical and Aeronautical Engineering, University of Pretoria
Degree:	Master of Engineering (Mechanical Engineering)

Sport Utility Vehicles are designed to be used on both smooth roads and rough off-road terrains. These vastly different operating conditions require vehicle and suspension parameters that lie at opposite ends of the design space. Harder suspension is required for adequate handling on smooth roads and softer suspension, combined with large ground clearance, allows for improved ride comfort and off-road capability. This causes a compromise in the suspension setup. As a result of the typically softer suspension, as well higher centre of gravity, compared to passenger vehicles, SUVs are more prone to rollover.

This motivates researchers to find methods of improving the handling of Sport Utility Vehicles, which in turn would decrease the number of rollover accidents involving these vehicles. The proposed methods include, amongst others, the use of active anti-roll bars, slow-active, semi-active and active suspension. The control strategies of most of these methods are based on the current vehicle state, giving them the same downfall, which is a delay in switching. To eliminate this delay, some type of preview is required.

A non-linear vehicle preview model that solves in real-time was developed and implemented on the Land Rover Defender 110. The vehicle preview model is capable of predicting vehicle states up to $300ms$ (limited by the current processor) with good accuracy. The predicted states can then be used as an input to a control system or the model can be used as a state estimator.

Even though there are numerous possible applications of the vehicle preview model, it was only implemented in one existing suspension control system, known as the Running Root Mean Square strategy. This strategy compares the measured lateral and vertical accelerations of the vehicle to decide on the suitable suspension setting. This strategy has a delay of about 290 ms.

When the predicted lateral acceleration was used as an input to the existing suspension control strategy, the delay in switching was reduced and improvements in vehicle handling of up to 56 % was achieved over a variety of tests.

ACKNOWLEDGEMENTS

I would like to thank:

- Prof. Els, for his support, guidance and the opportunity to be part of the Vehicle Dynamics Group
- Theunis Botha and Carl Becker, for always being willing to help (even on their own birthdays)
- My parents Leslie and Anneke Linström, for the opportunities, love and support
- My sister Lize Linström, for all the funny moments
- My grandmothers for always believing in me and all the Sunday lunches
- Olga Musienko, for all the love, patience and support throughout my studies
- My fellow students: Joachim Stallmann, Herman Hamersma, Vincent Wehrmeyer and Anria Strydom

TABLE OF CONTENTS

LIST OF FIGURES

LIST OF TABLES

LIST OF ABBREVIATIONS

CG	Centre of gravity
CPU	Central Processing Unit
DGPS	Differential Global Positioning System
DLC	Double Lane Change
DOF	Degrees Of Freedom
DRAM	Dynamic Random-Access Memory
FFT	Fast Fourier Transform
GAP	Genetic Algorithm Predictor
GPS	Global Positioning System
IMU	Inertial Measurement Unit
PC	Personal Computer
R^2	Coefficient Of Determination
RMS	Root Mean Square
RRMS	Running Root Mean Square
SUV	Sport Utility Vehicle
U.S.A.	United States of America
VBOX	Velocity Box
VPM	Vehicle Preview Model
$4S_4$	Four State Semi-Active Suspension System

LIST OF SYMBOLS

A	Area $[m^2]$
B	Stiffness Factor
C	Shape Factor
CG_l	Distance of CG to the left tyres $[m]$
CG_r	Distance of CG to the right tyres $[m]$
CG_{yoff}	CG offset from the centre line of the vehicle $[m]$
ΔCG_f	Change of CG position due to roll angle $[m]$
ΔCG_r	Change of CG position due to roll angle $[m]$
D	Peak Factor
d_f	Front Track Width $[m]$
d_r	Rear Track Width $[m]$
E	Curvature Factor
F_{damp}	Damping Force $[N]$
F_S	Suspension Force $[N]$
F_{Sl}	Sum of suspension forces on the left of the vehicle $[N]$
F_{Sr}	Sum of suspension forces on the right of the vehicle $[N]$
F_{lf}	Left front lateral tyre force $[N]$
F_{lr}	Left rear lateral tyre force $[N]$
F_{rf}	Right front lateral tyre force $[N]$
F_{rr}	Right rear lateral tyre force $[N]$
F_{sd}	Suspension force due to suspension displacement $[N]$
F_{slf}	Left front suspension force $[N]$
F_{slr}	Left rear suspension force $[N]$
F_{so}	Initial suspension force $[N]$
F_{srf}	Right front suspension force $[N]$
F_{srr}	Right rear suspension force $[N]$
F_y	Lateral tyre force $[N]$
F_{yl}	Sum of lateral forces of tyres on the left $[N]$
F_{yr}	Sum of lateral forces of tyres on the right $[N]$
F_z	Vertical tyre force $[N]$
F_{zlf}	Left front vertical tyre force $[N]$
F_{zlr}	Left rear vertical tyre force $[N]$
F_{zrf}	Right front vertical tyre force $[N]$

F_{zrr}	Right rear vertical tyre force $[N]$
ΔF_{zf}	Change in vertical force on front tyres $[N]$
ΔF_{zr}	Change in vertical force on rear tyres $[N]$
fit_1	Quadratic damping force fit 1
fit_2	Quadratic damping force fit 2
fit_3	Quadratic damping force fit 3
fit_4	Quadratic damping force fit 4
g	Gravitational Acceleration $[9.81\, m/s^2]$
h	Step size
h_{cg}	Centre of gravity height $[m]$
h_f	Roll centre height front $[m]$
h_r	Roll centre height rear $[m]$
I_x	Roll mass moment of inertia $[kgm^2]$
I_z	Yaw mass moment of inertia $[kgm^2]$
K_{sf}	Suspension stiffness front $[N/m]$
K_{sr}	Suspension stiffness rear $[N/m]$
$K_{\varphi f}$	Suspension roll stiffness front $[N/m]$
$K_{\varphi r}$	Suspension roll stiffness rear $[N/m]$
k	Constant
l_c	Distance from rear axle to Correvit $[m]$
l_f	Distance from front axle to centre of gravity $[m]$
l_r	Distance from rear axle to centre of gravity $[m]$
m	Mass of entire vehicle $[kg]$
m_b	Mass of vehicle body $[kg]$
M_x	Moment about longitudinal axis $[Nm]$
M_z	Moment about vertical axis $[Nm]$
n	Step number
P_{sd}	Suspension pressure due to suspension displacement $[Pa]$
P_{so}	Initial suspension pressure $[Pa]$
r	Yaw rate $[deg/s]$
$\dot{r}$	Yaw acceleration $[deg/s^2]$
R^2	Coefficient of determination
S_h	Horizontal shift for Magic Formula $[N]$
S_v	Vertical shift for Magic Formula $[N]$
s	Distance between suspension struts $[m]$

$susp_d$	$4S_4$ damper setting
t	Time $[s]$
t_s	Distance between suspension struts $[m]$
V	Speed $[m/s]$
V_{sd}	Suspension volume due to suspension displacement $[m^3]$
V_{so}	Initial suspension volume $[m^3]$
W_{lf}	Left front tyre vertical load $[N]$
W_{lr}	Left rear tyre vertical load $[N]$
W_{rf}	Right front tyre vertical load $[N]$
W_{rr}	Right rear tyre vertical load $[N]$
X	Unshifted side-slip angle $[deg]$
X_n	Vehicle parameters
x	Shifted side-slip angle $[deg]$
Y	Shifted tyre lateral force $[N]$
y	Unshifted tyre lateral force $[N]$
$\ddot{y}$	Lateral Acceleration$[m/s^2]$
z_s	Suspension displacement $[m]$
z_{slf}	Left front suspension displacement $[m]$
z_{slr}	Left rear suspension displacement $[m]$
z_{so}	Initial suspension displacement $[m]$
z_{srf}	Right front suspension displacement $[m]$
z_{srr}	Right rear suspension displacement $[m]$
$\dot{z}_s$	Suspension velocity $[m/s]$
$\dot{z}_{slf}$	Left front suspension velocity $[m/s]$
$\dot{z}_{slr}$	Left rear suspension velocity $[m/s]$
$\dot{z}_{srf}$	Right front suspension velocity $[m/s]$
$\dot{z}_{srr}$	Right rear suspension velocity $[m/s]$
β	Vehicle side-slip angle $[deg]$
β_{Cor}	Side-Slip angle at sensor $[deg]$
β_{lf}	Left front tyre side-slip angle $[deg]$
β_{lr}	Left rear tyre side-slip angle $[deg]$
β_{rf}	Right front tyre side-slip angle $[deg]$
β_{rr}	Right rear tyre side-slip angle $[deg]$
$\dot{\beta}$	Vehicle side-slip rate $[deg/s]$
γ	Gas constant [1.4]

δ	Steering angle $[deg]$
$\dot{\delta}$	Steering rate $[deg/s]$
τ	Preview time $[ms]$
φ	Roll angle $[deg]$
$\dot{\varphi}$	Roll rate $[deg/s]$
$\ddot{\varphi}$	Roll acceleration $[deg/s^2]$

1 INTRODUCTION

Sport Utility Vehicles (SUVs) have grown in popularity over the past years and even though these vehicles are designed for off-road conditions, most SUVs never get off the beaten track. 39% of Americans feel more powerful when driving a SUV and 50% do not consider that loading the vehicle increases the risk of rollover (Governor's Office of Consumer Affairs, 2005).

SUVs have a higher ride height and softer suspension than most passenger cars, making them better equipped for rough off-road conditions. The combination of a higher ride height and softer suspension make SUVs more prone to rollover than passenger cars.

In the U.S.A. 33% of vehicle accident fatalities are due to vehicles that roll, while vehicle rollover only amounts to 2.3% of all types of accidents (Strashny, 2007). In South Africa in 2009, 24% of the total number of accidents were rollover related and contributed 25% to the total number of fatalities (second to pedestrian related accidents at 28%). Rollover accidents had a severity rate of 1.32 fatalities per accident (Road Traffic Management Corporation, 2009). It can be seen that vehicle rollover is a serious type of accident and that many SUV occupants lose their lives due to rollover.

Figure 1-1 shows the number of fatalities due to rollover per million registered vehicles. SUVs have the highest rate of fatalities (Dukkipati et al, 2008).

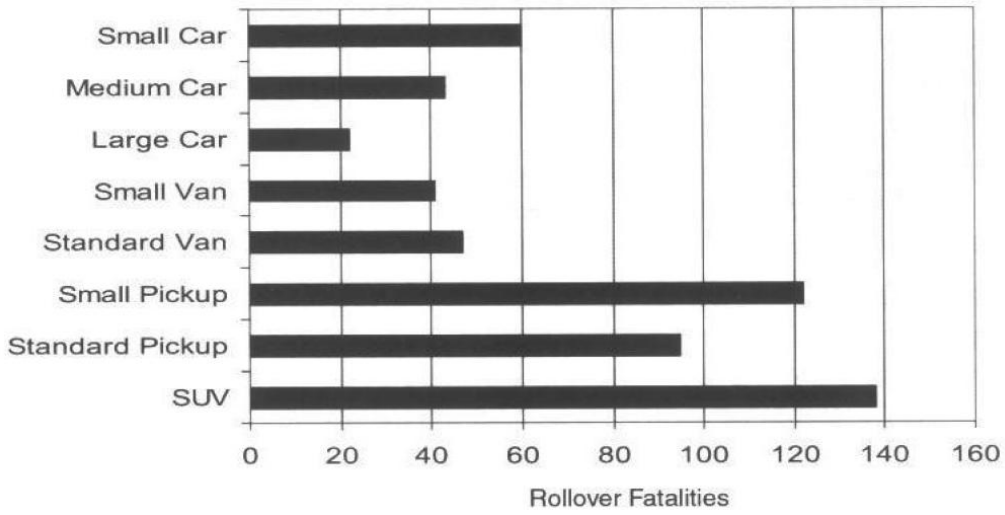

Figure 1-1: Rollover Fatalities (Dukkipati et al, 2008)

These disturbing statistics motivate researchers to find methods of improving the handling of SUVs and decreasing the number of rollover accidents involving these vehicles. Proposed methods include, amongst others, the use of active anti-roll bars, slow-active, semi-active and active suspension as well as brake-based stability control systems. The control strategies of most of these

methods are based on the current vehicle state, giving them a similar downfall, which is a delay in switching.

A control system implemented on a vehicle goes through different steps before the output has any effect on the dynamics of the vehicle. The control system (Figure 1-2) can be anything from a human driver to a driver assist system implemented on the vehicle. The inputs need to be processed to make the required decision and send out the necessary control signals to the actuators. All of this contributes to the total delay of the system. The output signal is sent to the actuator on the vehicle, which creates a further delay that depends on the actuator response time. The final delay is due to the amount of time required for the vehicle to respond to these changes. In many of these steps, sensor data is filtered to decrease noise, causing additional delays.

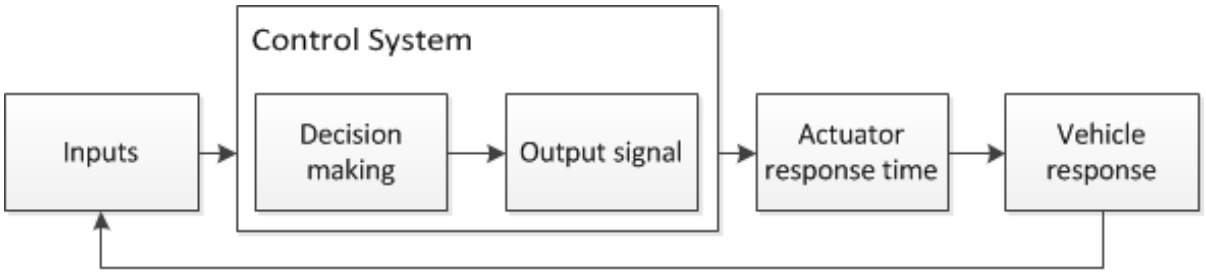

Figure 1-2: Control System Delay

Consider a human driver that controls the lateral motion of a vehicle as an example. Firstly, the human senses an obstacle in the road ahead; the human then makes the decision whether to avoid the obstacle on the left hand side or on the right hand side, and then makes the required changes to the steering wheel, brakes etc. The brain takes time to process the data and to send signals to the limbs (actuators). Once the human has turned the steering wheel, there is a further delay before the vehicle can change direction, as the tyres need time to generate the required forces to accelerate the vehicle in the intended direction. All of these phases contribute to the delay present in most control systems. If some sort of preview could be implemented to reduce or eliminate these delays, many vehicle control systems can benefit.

Preview models allow the control systems to predict the future state of the vehicle and make control decisions using the predicted states. Some vehicle preview systems used and developed in the past include convoy preview and steering preview based on a Global Positioning System. Research has also been done on rollover threat, rollover warning and time to rollover.

The aim of this study is to develop and validate a real-time non-linear vehicle preview model that predicts certain vehicle states based on the current vehicle state.

2 LITERATURE SURVEY

To formulate the research question, a literature review was done to understand the problems related to SUVs and to identify solutions suggested in the past. The literature includes a study on the ride comfort vs. handling compromise to understand where typical SUV related problems originate and on control strategies that have been implemented in the past to improve the handling of the vehicle.

2.1 Ride Comfort vs. Handling Compromise

SUVs are designed to be used on smooth roads at high speeds as well as under rough off-road conditions. Having a vehicle that accommodates this variety of terrains creates a compromise between the ride comfort, handling and rollover propensity of the vehicle.

Ride comfort for rough off-road conditions requires a soft suspension setup and a higher CG for more ground clearance, but this setup jeopardizes the handling of the vehicle. The ideal suspension for handling is much harder, and allows the vehicle to negotiate corners at high speeds with little body roll.

2.2 Methods to reduce the ride vs. handling compromise

Different possibilities exist to reduce the ride vs. handling compromise. A few will discussed below.

Yi et al (2007) suggested a model-based roll state estimator that can be used to detect impending rollover. A vertical dynamics model-based estimator is used to estimate the roll motion caused by road disturbances by measuring the accelerations of the sprung and unsprung masses. Measuring the lateral acceleration and the yaw rate of the vehicle, a lateral dynamics model-based estimator is used to estimate the roll motion caused by the lateral movement of the vehicle. Using these two estimators together, it was shown in simulation that the roll angle, roll rate and rollover index are accurately estimated to prevent vehicle rollover.

Chen and Peng (2001) used differential braking of SUVs to try to prevent vehicle rollover based on the time to rollover metric. A vehicle model of a Jeep Cherokee was used in simulation to show that the anti-rollover control system improved the performance for all the tests conducted. When tests were performed with a human driver in-the-loop, it was found that the performance of the model deteriorated and that much larger load transfer was experienced.

Els (2006) investigated the ride comfort vs. handling compromise for off-road vehicles. A semi-active suspension system was developed, manufactured and implemented on a Land Rover Defender 110 known as the Four State Semi-Active Suspension System ($4S_4$). The $4S_4$ is able to switch between two discrete spring characteristics and two discrete damper characteristics that were optimised for ride comfort and for handling respectively. The ride comfort of the vehicle was optimised by minimising the vertical acceleration of the vehicle whereas the handling was optimised by minimising the body roll angle.

The philosophy behind the $4S_4$ suspension system is that it will mostly operate in ride comfort mode. Switching to handling mode is only done when required and usually only for short periods of time until the handling manoeuvre is completed. The circuit diagram for the $4S_4$ can be seen in Figure 2-1.

When Valve 3 is closed, the system is operating on one accumulator (Accumulator 1), resulting in a high spring rate. When Valve 1 is closed, the fluid is forced through Damper 1, which gives high damping. When Valve 1 is opened, a bypass channel is created and the damping is low.

When Valve 3 is opened the hydropneumatic spring uses both Accumulator 1 and Accumulator 2. This means that the total gas volume is increased, and as a result a low spring rate is achieved. Closing Valves 1 and 2 results in high damping and vice versa. The system is also fitted with a pump and outlet valve so that the ride height can be adjusted.

High and low spring rates can be tuned independently by changing the gas volume of the two accumulators. The high damping characteristics are determined by the characteristics of Damper 1 and 2, while the low damping is determined mainly by the flow resistance through the bypass valves and channels.

Switching between ride comfort and handling mode typically takes 50 to 90 ms based on the operating conditions due to the response time of the hydraulic valves used.

The final design was manufactured by Els (2006) and can be seen in Figure 2-2. The suspension unit can be seen fitted to the vehicle in Figure 2-3 and Figure 2-4.

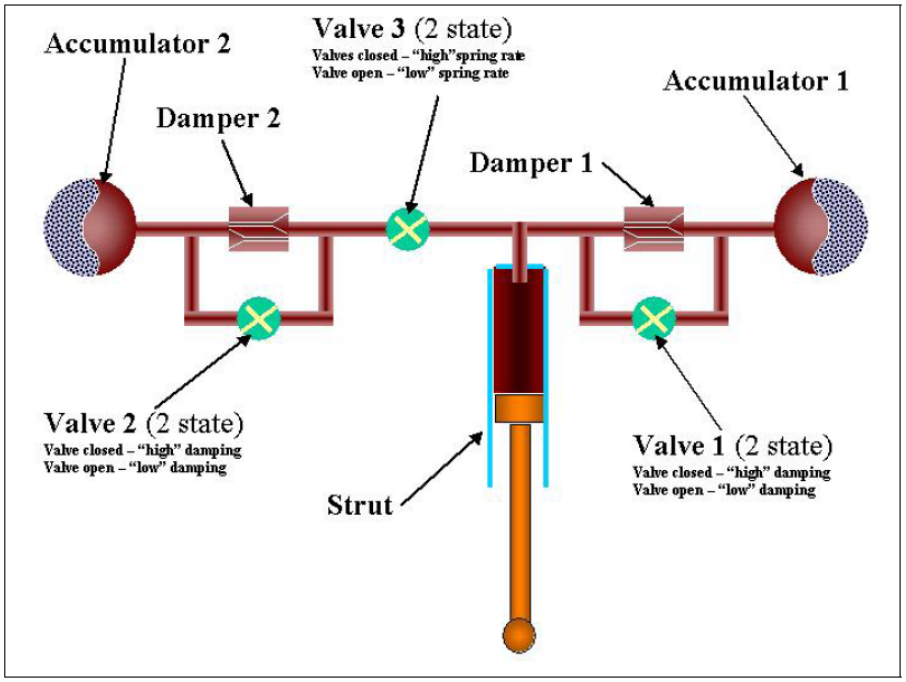

Figure 2-1: $4S_4$ circuit diagram Els (2006)

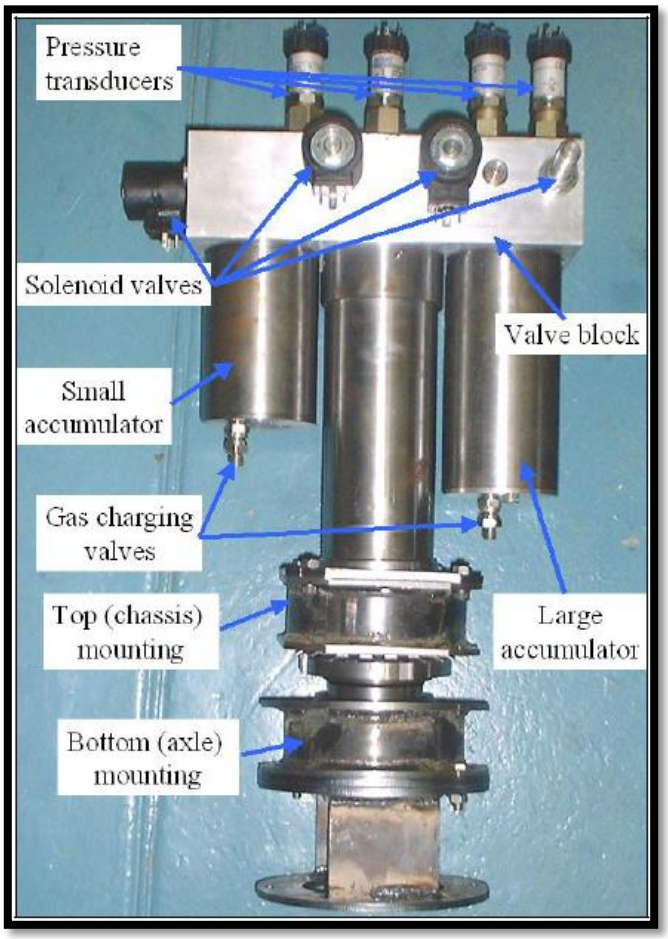

Figure 2-2: $4S_4$ unit (Els, 2006)

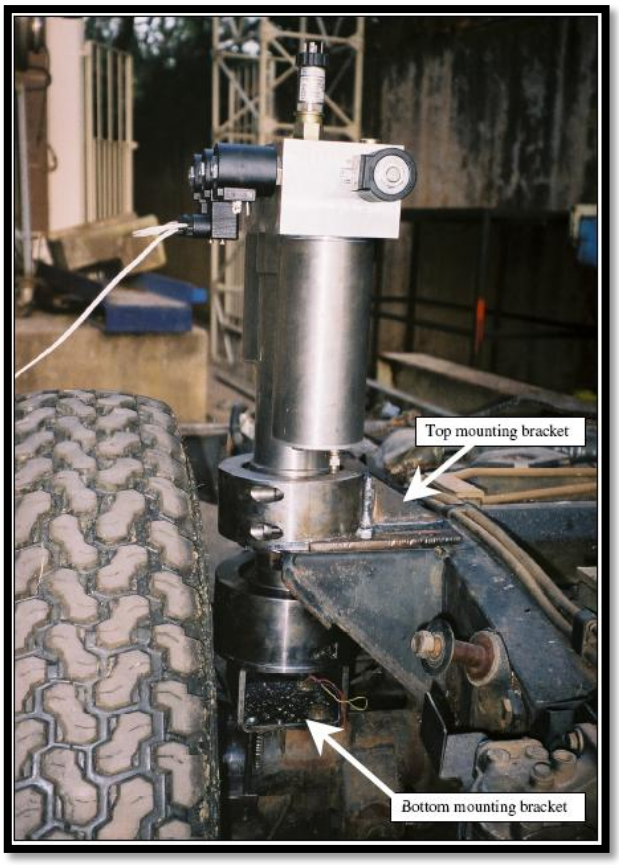

Figure 2-3: Right rear suspension fitted to chassis - front view (Els, 2006)

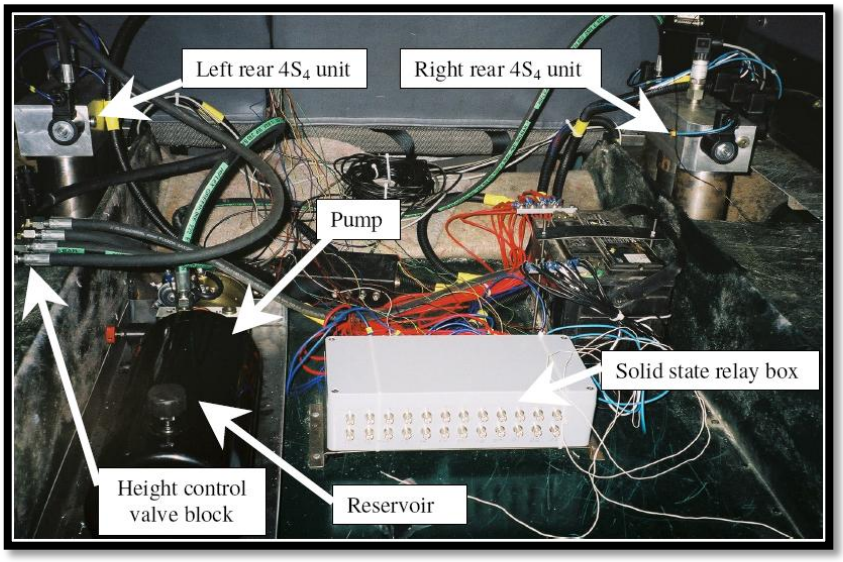

Figure 2-4: Piping, wiring and electronics (Els, 2006)

The current vehicle has three user input options for suspension settings. The first option is called the ride comfort mode and switches the $4S_4$ to the soft suspension mode that has been optimised to improve the ride comfort under off-road conditions. The second option is called the handling mode

that switches the $4S_4$ to the hard suspension mode that has been optimised to improve the handling ability of the vehicle.

The final setting is referred to as the Running Root Mean Square (RRMS), which compares the average absolute values of the vertical acceleration to the lateral acceleration by using 100 points at a sampling frequency of 100 Hz. It switches to handling mode when the lateral acceleration RRMS exceeds the vertical acceleration RRMS and to ride mode when the vertical acceleration RRMS exceeds the lateral acceleration RRMS.

It was concluded, after thoroughly testing the vehicle using many different switching strategies, that the RRMS strategy appeared to work well for most test conditions. One of the drawbacks of the RRMS is the delay in switching. This is understandable as the lateral acceleration changes very quickly during a double lane change, and because the lateral acceleration RRMS value over a 1 second period is used, it takes some time before this increase is detected.

Referring back to Figure 1-2, the vertical and lateral accelerations are measured and their RRMS values are calculated and compared to one another. This causes a delay of about 300 ms for a 1 second RRMS comparison, implemented by Els (2006), as shown in Figure 2-5. After making the ride vs. handling decision, the signal that triggers the valves in the suspension is sent, adding to the total delay of the system. Once the valves receive the signal they have to switch, which takes between 50 to 90 ms based on the operating conditions, only then will the dynamics of the vehicle start changing. All these factors contribute to the total switching delay of the $4S_4$.

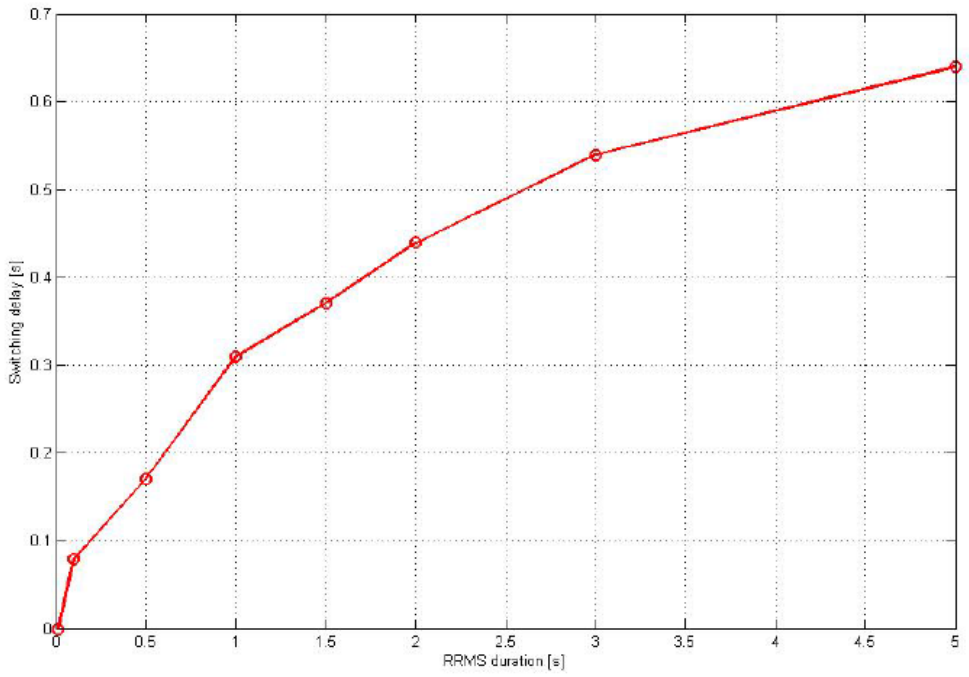

Figure 2-5: Effect of number of points in the RRMS on the switching delay for handling tests (Els, 2006)

Cronje and Els (2009) developed an active anti-roll bar and implemented it on the Land Rover Defender 110 in combination with the $4S_4$. The results show an improvement in the handling of the vehicle with little effect on the ride comfort. Steady-state handling tests showed that the vehicle roll angle was successfully eliminated up to the user defined 0.4g. The strategy also showed improvements of between 40% and 74% in the roll angle of the vehicle during dynamic handling tests.

Van der Westhuizen and Els (2012) replaced the active anti-roll bar used by Cronje and Els (2009) with slow active suspension control to reduce the risk of vehicle rollover by controlling the amount of oil in each of the $4S_4$ hydropneumatic suspension struts. By reducing the body roll angle of the vehicle, the load transfer is increased, which in turn will decrease the lateral forces generated by the tyres. This causes the vehicle to slide rather than roll, which in most cases is a safer option for the occupants in the vehicle.

To achieve good control results, the sensor signals had to be filtered using a low pass filter that created a delay of 90 ms. Oil flow limitations created a further delay limiting the band width of the system. Although the system was effective, it could be improved significantly by reducing the delays due to filtering and actuator response.

2.3 Preview Information

All the strategies discussed above rely on the current or past vehicle state measurements. This causes a delay, and if preview information were available, the performance of all of these strategies could be improved. Instead of trying to recover a vehicle from a dangerous state, the dangerous state can be avoided.

Trent and Greene (2002) developed a model-based genetic algorithm predictor (GAP) that was used to predict the potential for vehicle rollover. The model was developed for a 1997 Jeep Cherokee. Assuming that all operating conditions remain constant, the GAP is used to determine the system input (tyre deflection) that will result in vehicle rollover. Using simulations, it was shown that the vehicle rollover can be predicted by up to 400 ms.

Yim (2011) designed a preview controller to prevent vehicle rollover by assuming that the driver's steering input can be previewed by means of a Global Positioning System and an Inertial Measurement Unit. A linear vehicle model with active suspension and differential braking was used in simulation to show that a linear quadratic static output feedback control strategy performed well at preventing rollover by reducing the roll angle and lateral acceleration of the model.

Lateral preview type models have also been used in developing vehicle driver models (Ungoren and Peng, 2005).

2.4 Problem Statement

If a vehicle preview model (VPM) could be developed, the possible applications of such a model are numerous. The model would be able to predict different vehicle states that could be used with the suggested strategies to make SUVs safer vehicles. Even if the preview time is not enough for the human driver to react, the time should be sufficient for driver assist systems to make the necessary changes.

Some suspension switching strategies have similar downfalls, being that there is a delay in the switching time, as the strategies are based on measurements made of the present vehicle state. The preview strategies have been implemented on vehicle simulation models (Trent and Greene, 2002) and linear vehicle models (Yim, 2011), but implementing it on a test vehicle seems rare, as it presents numerous problems, including some states that can't be measured effectively as well as the noisy nature of the measurements.

In this study a validated VPM will be developed and implemented in real-time on a Land Rover Defender 110 SUV. The preview model outputs will be used to improve the existing RRMS ride vs. handling strategy currently used on the test vehicle at the University of Pretoria. The research question is stated as follows:

"Could a VPM be used to predict the lateral acceleration of the vehicle to reduce or eliminate the switching delay of the RRMS strategy and improve the handling of the vehicle?"

2.5 Project Plan

The research question has now been defined after looking at the literature. The following steps will be followed to find a suitable solution to the problem:

- Develop and validate a simulation model for the test vehicle.
- Develop a vehicle preview model and validate the model using simulations as well as experimentally obtained data.
- Implement the model in real-time on a test vehicle and ensure the model performance is satisfactory.
- Solve any problems caused by using noisy real-time measurements.
- Determine the improvement in handling obtained by using the VPM predictions to make the ride comfort vs. handling decision.
- Thoroughly test the model in different driving conditions to ensure all-round satisfactory performance.

3 THE VEHICLE AND VEHICLE MODEL

This chapter discusses the test vehicle and the validation of the vehicle simulation model.

3.1 The Test Vehicle

The test vehicle is a Land Rover Defender 110 as seen in Figure 3-1 and has been used at the University of Pretoria for many years. Over the years, numerous modifications have been made. The vehicle is fitted with the $4S_4$ that switches between "ride comfort" mode and "handling" mode as discussed in Section 2.2. The vehicle is also fitted with several sensors used for measurement and control. The vehicle falls under the category of a SUV and suffers from all the typical SUV related problems such as a high CG, soft suspension, high profile tyres etc.

Figure 3-1: Land Rover Defender 110

3.2 ADAMS model

Being able to use a validated model for simulations (instead of experimental tests) is a more economical way of developing, testing and fine tuning any new systems or control strategies that need to be implemented. In the simulation stages of model development the user can make numerous alterations to the model and test them using little resources at low risk.

Over the years a 15 degrees of freedom (DOF) non-linear vehicle model of the Land Rover Defender 110 has been developed in ADAMS, as seen in Figure 3-2. The original model was

developed by Thoresson (2007) and over the years many changes have been made. The most recent ADAMS model includes the non-linear $4S_4$ suspension setup developed by Els (2006). The model uses the Pajecka 89 tyre model, which will be explained in more detail later.

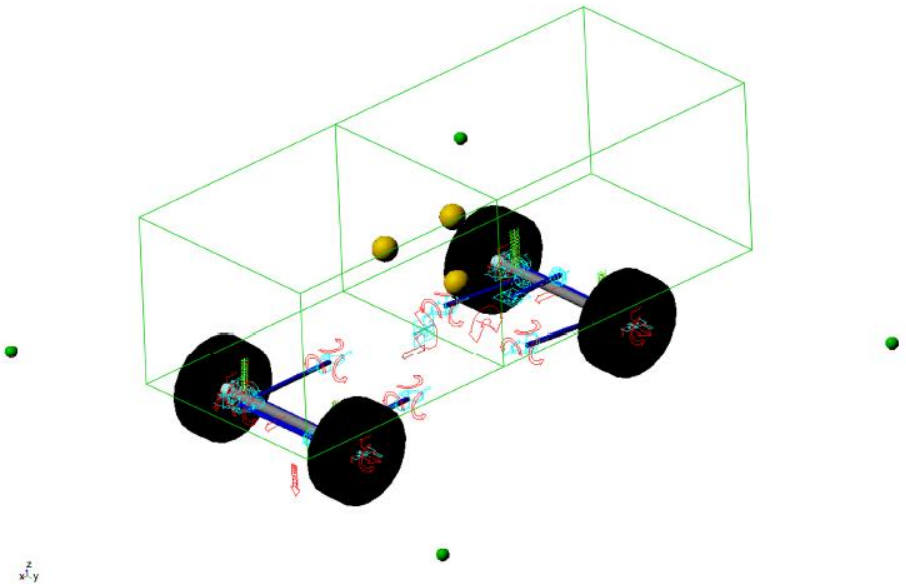

Figure 3-2: Graphical view of the vehicle modelled in ADAMS (Botha, 2011)

The modelled front suspension can be seen in Figure 3-3, showing all the connections and reaction forces used. The front suspension is modelled as a rigid axle that is connected to the chassis via two leading arms. In order to prevent the wheels from moving laterally, the axle is connected to the body via a Panhard rod.

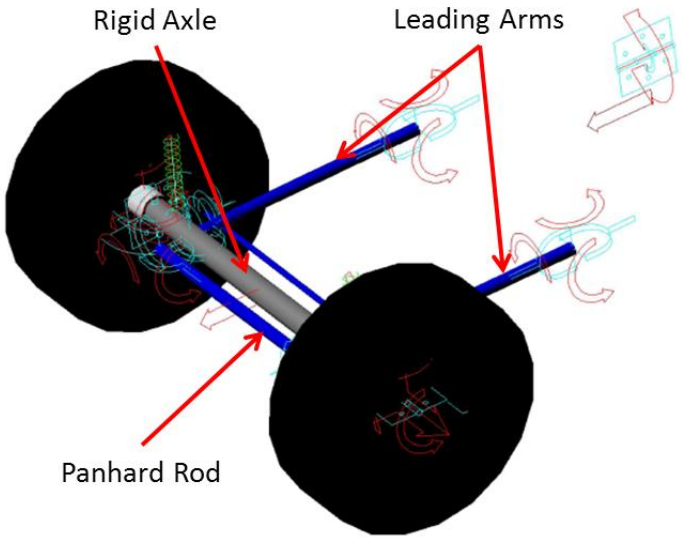

Figure 3-3: Front suspension of the vehicle modelled in ADAMS. (Adapted from Botha, 2011)

The rear suspension (Figure 3-4) is modelled using a rigid axle connected to the chassis using two trailing arms. To keep the rigid axle from moving in the lateral direction it is connected to the chassis via an A-arm.

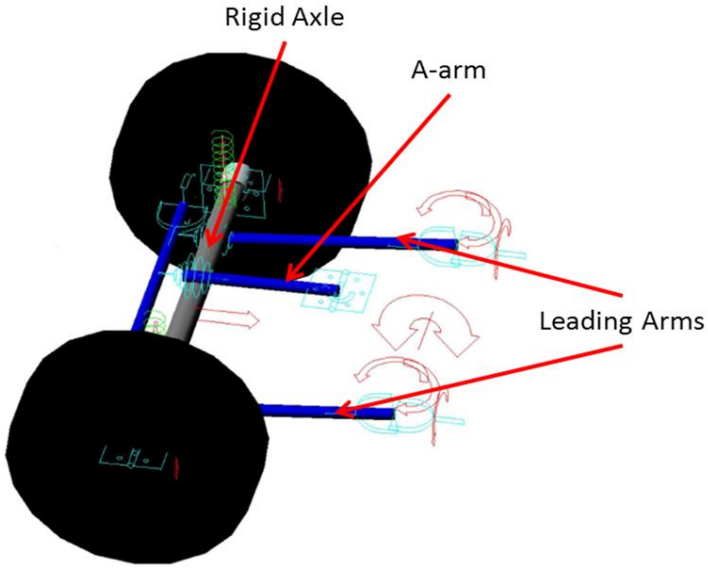

Figure 3-4: Rear suspension of the vehicle modelled in ADAMS. (Adapted from Botha, 2011)

All the control systems are modelled using Simulink and MATLAB with ADAMS co-simulations. This allows for easy modification and modelling of all the processes and controls required. The current steering driver model used for path following in ADAMS was developed and implemented by Botha (2011).

3.2.1 Measurement Instrumentation

Table 3-1 lists the sensors/instruments implemented on the vehicle that are used to capture data. The measurements are initially used for validation and later the same measurements are used as inputs to the VPM.

The steering angle is measured with a potentiometer installed on the kingpin of the right front wheel. From the measured steering angle (δ) the steering rate $(\dot{\delta})$ is calculated using the backwards differencing method as in Equation 3.1.

$$\dot{\delta}(i) = \frac{\delta(i) - \delta(i-1)}{t(i) - t(i-1)} \tag{3.1}$$

The side-slip angle is measured using the Correvit S-HR sensor that is mounted at the rear of the vehicle as seen in Figure 3-5. Since mounting it on the CG of the vehicle is not possible the measured side-slip angle values (β_{Cor}) need to be transferred to the CG of the vehicle. Referring to Figure 3-6

the vehicle side-slip angle is calculated from the Correvit S-HR measurement using Equation 3.2 in a similar way to how Abe (2009) calculates the side-slip angle at each tyre.

$$\beta \approx \frac{V\beta_{Cor} + (l_r + l_c)r}{V} \tag{3.2}$$

Table 3-1: Instruments on Vehicle

Vehicle Parameter	Instrument
Vehicle Speed	Racelogic Velocity BOX 3 (VBOX3) Differential Global Positioning System (DGPS)
Steering Angle	Potentiometer
Side-slip Angle	Correvit S-HR
Roll Angle	2x Acuity AR700 Laser Displacement Sensors
Roll Rate	Solid state gyroscope (CRS03)
Yaw Rate	Solid state gyroscope (CRS03)
Lateral Acceleration	Accelerometer (Crossbow 4g)
Vertical Acceleration	Accelerometer (Crossbow 4g)
GPS Coordinates	Racelogic Velocity BOX 3 (VBOX3) Differential Global Positioning System (DGPS)

Figure 3-5: Correvit S-HR Mounted to Vehicle

The roll angle is measured using two Acuity AR700 laser displacement sensors mounted on both sides of the vehicle. By measuring the two displacements and knowing exactly where the lasers are

positioned on the vehicle the roll angle can be calculated. Figure 3-7 shows one of the lasers mounted on the right hand side of the vehicle.

The roll rate and yaw rate is measured using a solid state gyroscope (CRS03) mounted inside the vehicle and the vertical and lateral accelerations are measured using a Crossbow 4g accelerometer that is mounted approximately at the CG position of the vehicle.

During testing of the vehicle, dangerous manoeuvres are performed and to ensure the safety of the occupants in the vehicle and to prevent vehicle rollover, outriggers are mounted to the vehicle. The outriggers can be seen in Figure 3-7.

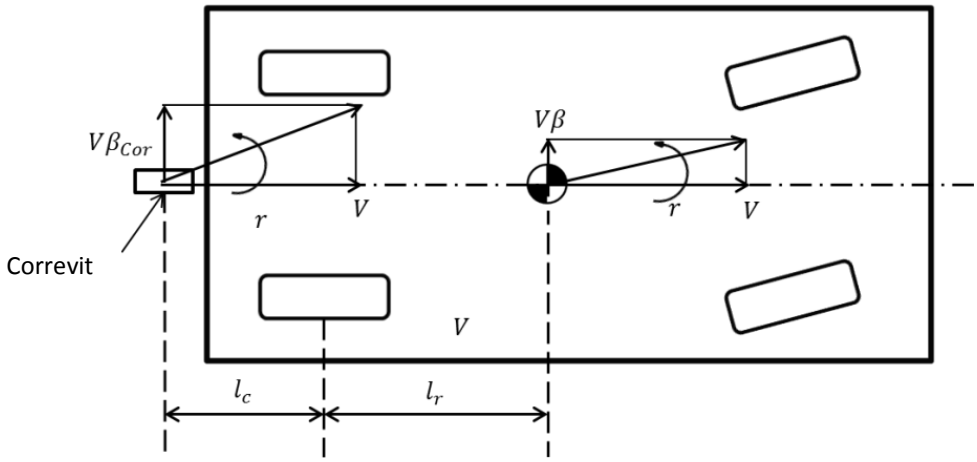

Figure 3-6: Moving Correvit S-HR Side-Slip to CG

Figure 3-7: Acuity Lasers and Outriggers on Vehicle

3.2.2 ADAMS Model Validation

To use the ADAMS vehicle model in developing a preview model, it needs to be validated for handling. This would include the validation of side-slip angle, yaw rate, roll rate, roll angle and lateral acceleration.

Experimentally obtained data is compared to simulation results for validation of the ADAMS model. This is done by performing double lane change (DLC) tests (International Organisation for Standardisation, 1999) at 49, 61, 70 and 78 km/h. In Figure 3-8 the measured results are plotted in blue and the simulation results are plotted in red for a DLC performed at 70 km/h.

Table 3-2 shows the coefficient of determination (R^2) for the measured results compared to the simulation results. When looking at the R^2 values it is clear that the ADAMS vehicle model accurately simulates the path, side-slip angle, yaw rate, roll angle and lateral acceleration. This is not the case for the roll rate as unknown friction forces in the suspension system have a major effect on the vehicle roll dynamics. These forces have not yet been accounted for in the model.

The discrepancies between the measured and simulated results are not only caused by the vehicle simulation model, but also by the path following driver model that is used.

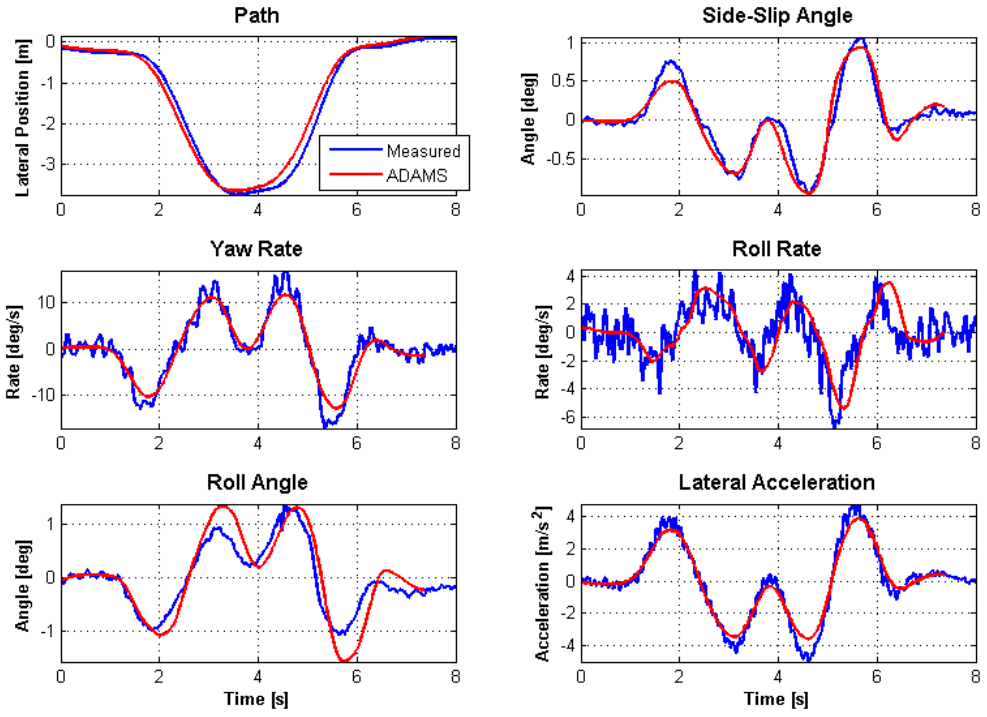

Figure 3-8: DLC at 70 km/h ADAMS Validation

Table 3-2: Coefficient of Determination ADAMS Validation

	Coefficient of Determination (R^2)					
Speed [km/h]	**Path**	**Slip-angle**	**Yaw Rate**	**Roll Rate**	**Roll Angle**	**Lateral Acc**
49	0.99	0.84	0.91	0.17	0.65	0.95
61	0.98	0.84	0.92	0.42	0.80	0.96
70	0.98	0.93	0.92	0.48	0.76	0.96
78	0.96	0.91	0.90	0.59	0.67	0.97

3.3 Conclusion

The ADAMS vehicle model was successfully validated for handling using experimentally obtained data making it a good platform for the development and testing of a VPM. Once the VPM has been developed using ADAMS, it can be implemented on the test vehicle.

4 VEHICLE PREVIEW MODEL

This chapter is aimed at developing and validating a non-linear VPM capable of predicting the vehicle state at some time in the future based on the current vehicle state. Using these predicted vehicle states, the severity of a future manoeuvre, which may result in loss of control or stability of the vehicle (such as vehicle rollover), can be analysed and the necessary precautionary measures taken in advance to improve the safety of the occupants in the vehicle. The preview information can also eliminate or reduce the time delay present in many vehicle control systems.

To achieve computational efficiency for real-time implementation, a simplified vehicle model is required. The proposed model considers the lateral, yaw and roll dynamics of the vehicle body making it a 3-DOF model.

The VPM makes the following assumptions:

- The vehicle is driving at constant longitudinal speed (V) on a smooth surface.
- No aerodynamic or rolling resistance forces are considered.
- Only the lateral load transfer is considered.
- The CG of the vehicle remains fixed with respect to the vehicle and loading the vehicle with passengers or luggage has a negligible on the position of the CG.
- Only the tyre lateral force is taken into account and not the self-aligning torque. The model does include the longitudinal component of the lateral force generated by the tyres.
- Tyre deflection has no effect on the roll angle of the vehicle.
- The roll angle at the front axle equals the roll angle at the rear axle.
- The steer rate remains constant for the entire preview time period.

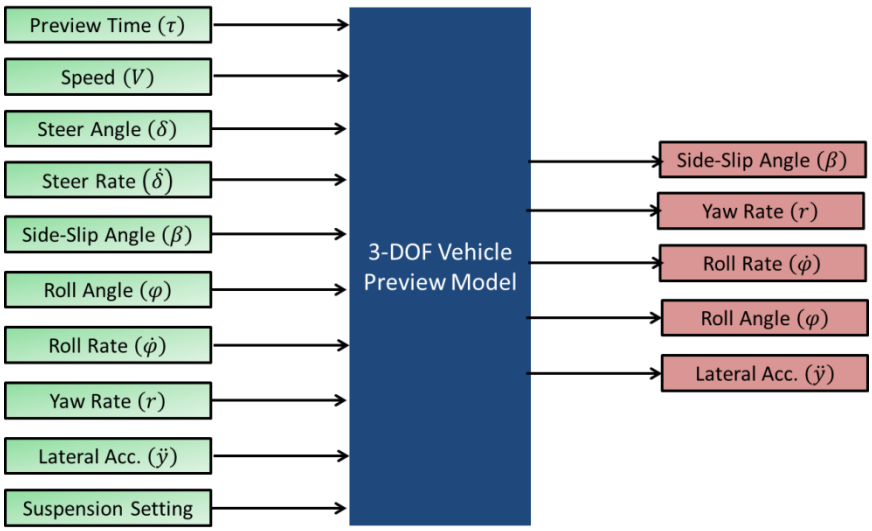

Figure 4-1: VPM Overview

The proposed VPM requires 10 inputs to predict 5 future states (Figure 4-1) and uses the Runge-Kutta method that will be discussed in Paragraph 4.1.7.

4.1 Simplified Vehicle Model

The only forces considered between the vehicle and environment are the vertical and lateral tyre forces as well as gravity. The tyres generate the required lateral forces $(F_{lf}, F_{rf}, F_{lr}, F_{rr})$ that enable the driver to control the vehicle. The tyre forces will be discussed in more detail in Paragraph 4.1.2.

Referring to the yaw-plane representation of the vehicle in Figure 4-2, the lateral motion and the yaw moment caused by the tyre lateral forces about the CG of the vehicle can be described as in Equation 4.1 and Equation 4.2, respectively as defined by Abe (2009).

$$\sum F_y = m\ddot{y} = mV(\dot{\beta} + r) = F_{lf} + F_{rf} + F_{lr} + F_{rr} \tag{4.1}$$

$$\sum M_z = I_z\dot{r} = l_f(F_{lf} + F_{rf}) - l_r(F_{lr} + F_{rr}) \tag{4.2}$$

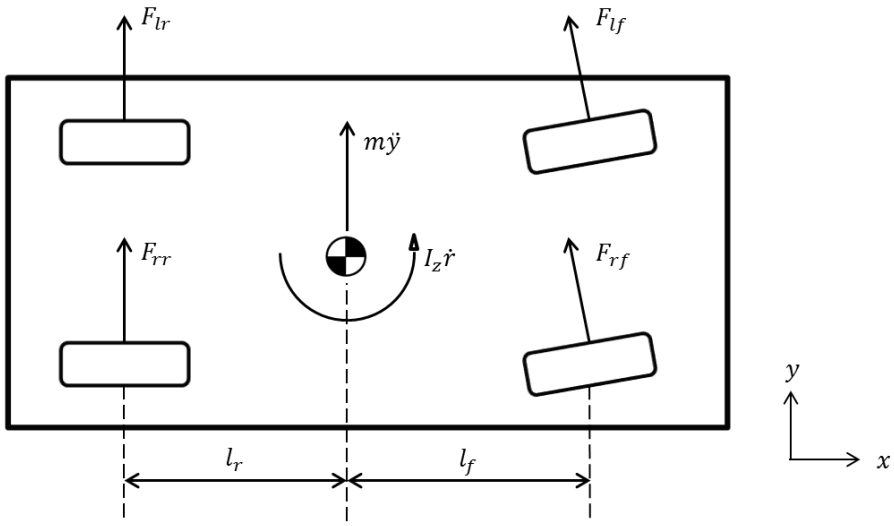

Figure 4-2: Top view for vehicle lateral and yaw motion

Similarly, from the roll-plane representation in Figure 4-3, the roll motion of the vehicle is described in Equation 4.3 by taking the sum of the moments about the CG of the vehicle. F_{Sl} and F_{Sr} are the sum of the suspension forces, while F_{yl} and F_{yr} are the sum of the tyre lateral forces on the left and the right of the vehicle, respectively.

$$\sum M_x = I_x\ddot{\varphi} = (F_{Sl} - F_{Sr})\frac{t_s}{2} + h_{cg}(F_{yl} + F_{yr}) \tag{4.3}$$

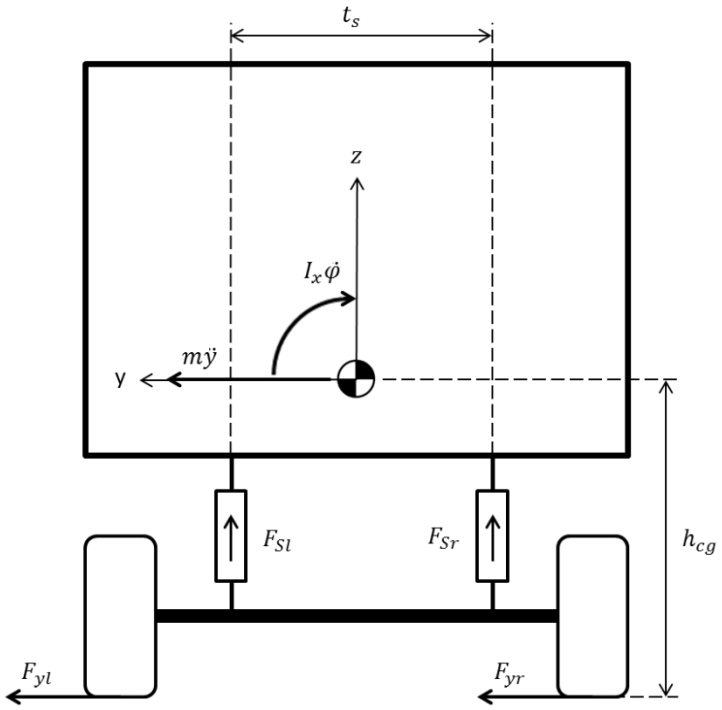

Figure 4-3: Rear view for roll motion

4.1.1 Vehicle Lateral Acceleration

The vehicle lateral acceleration is not solved as part of the differential equations, but gets updated at each iteration using the predicted lateral forces generated by the tyres (Figure 4-4). The lateral acceleration function uses the lateral tyre forces generated at each tyre to calculate the lateral acceleration output as in Equation 4.4 (Figure 4-3).

$$\ddot{y} = \frac{(F_{yl} + F_{yr})}{m} \tag{4.4}$$

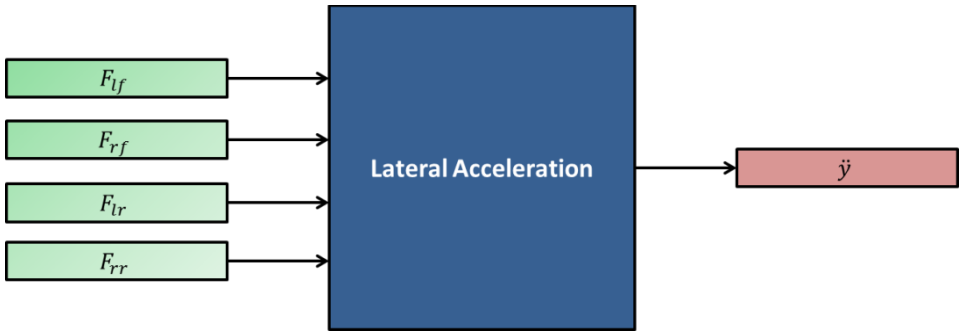

Figure 4-4: Lateral Acceleration

4.1.2 Tyre Lateral Force

Between each tyre and the road a lateral force that is a function of the vertical load and side-slip angle is genereated. Tyre forces are important as they are the only means of contact that the vehicle has with the road. Accurately modelling these forces is critical to achieving a vehicle model with acceptable accuracy.

To calculate the lateral tyre force generated by each tyre, the side-slip angle and vertical force of the tyre is required. The tyre lateral force function requires eight inputs and solves for four outputs as shown in Figure 4-5.

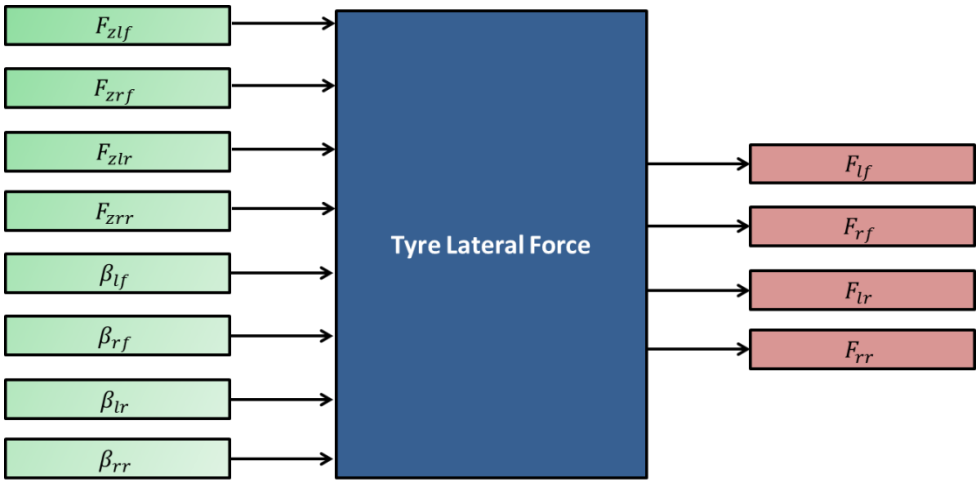

Figure 4-5: Tyre Lateral Force

One well known method of modelling the lateral tyre force is known as the Magic Formula developed by Pacjeka. The '89 model (Pacejka et al., 1989) is used for the VPM. Experimentally obtained lateral force vs. side-slip angle data at different vertical loads is required to implement the Magic Formula. A smooth curve is fitted through the data points, giving a full representation of the relationship between the side-slip angle and the lateral force for different vertical loads, as shown in Figure 4-6.

The Magic Formula is defined as follows (Pacejka et al., 1989):

$$y(x) = D\sin\left(C\arctan\left\{Bx - E\left(Bx - \arctan(Bx)\right)\right\}\right) \tag{4.5}$$

$$Y(X) = y(x) + S_v \tag{4.6}$$

$$x = X + S_h \tag{4.7}$$

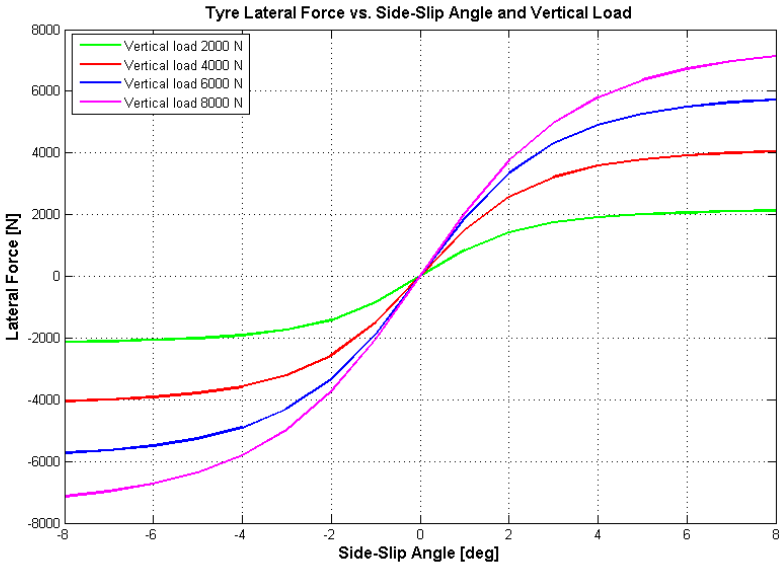

Figure 4-6: Tyre lateral force vs. side-slip angle and vertical load

4.1.3 Tyre Side-Slip Angle

The tyre side-slip angle is one of the states required to calculate the lateral tyre force. The tyre side-slip angle function requires four inputs and solves for the side-slip angle at each tyre as shown in Figure 4-7.

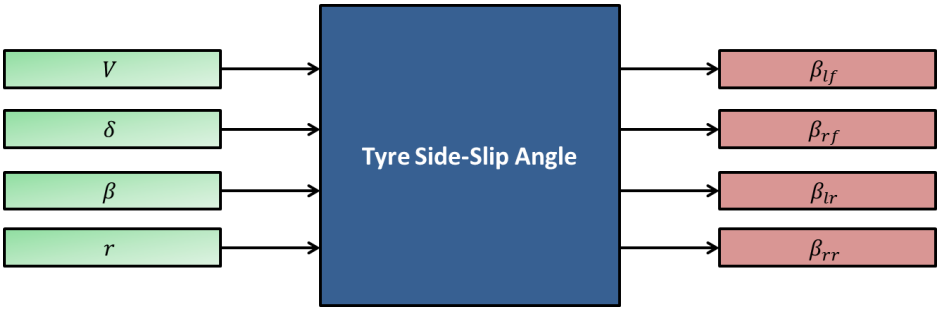

Figure 4-7: Tyre Side-Slip Angle

The lateral motion of a vehicle with front wheel steer is controlled by the driver applying a steer angle δ to the front wheels. The steer angle causes the tyres to deform, creating the required forces between the tyre and the road. The deformation results in a difference between the tyre heading and the tyre's centre line known as the side-slip angle (β) as shown in Figure 4-8.

The steer angle input causes a body side-slip angle at the centre of the vehicle as well as a side-slip angle at each tyre as shown in Figure 4-9. The side-slip angle at each tyre is calculated using Equation 4.8 to 4.11 as defined by Abe (2009).

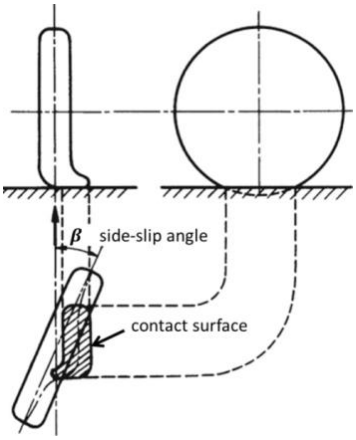

Figure 4-8: Tyre deflection with side slip (Abe, 2009)

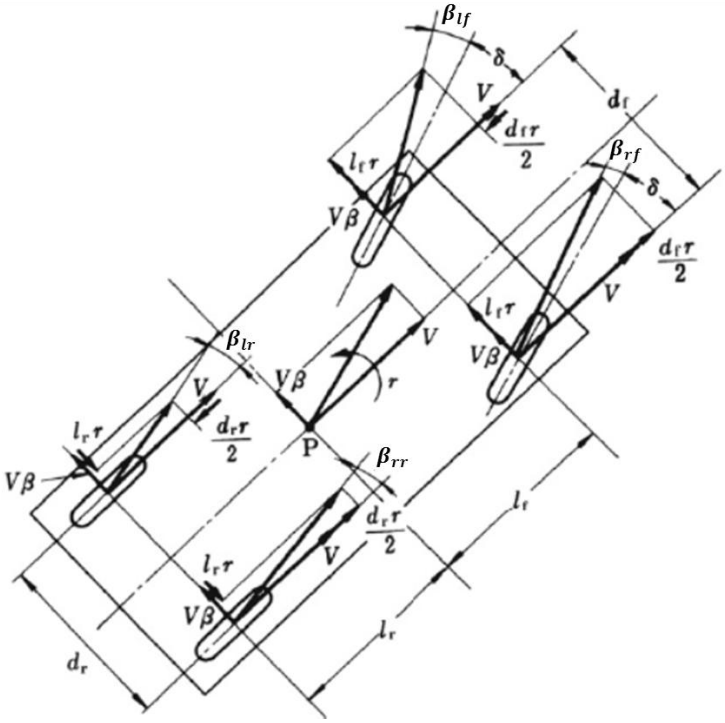

Figure 4-9: Tyre Side-Slip Angle (Abe, 2009)

$$\beta_{lf} \approx \frac{V\beta + l_f r}{V - d_f r/2} - \delta \tag{4.8}$$

$$\beta_{rf} \approx \frac{V\beta + l_f r}{V + d_f r/2} - \delta \tag{4.9}$$

$$\beta_{lr} \approx \frac{V\beta - l_r r}{V - d_r r/2} \tag{4.10}$$

$$\beta_{rr} \approx \frac{V\beta - l_r r}{V + d_r r/2} \tag{4.11}$$

4.1.4 Load Transfer

The last parameter still required to calculate the lateral tyre force is the vertical load at each tyre. This is calculated using the load transfer function which requires three inputs and solves for the vertical force at each tyre as shown in Figure 4-10.

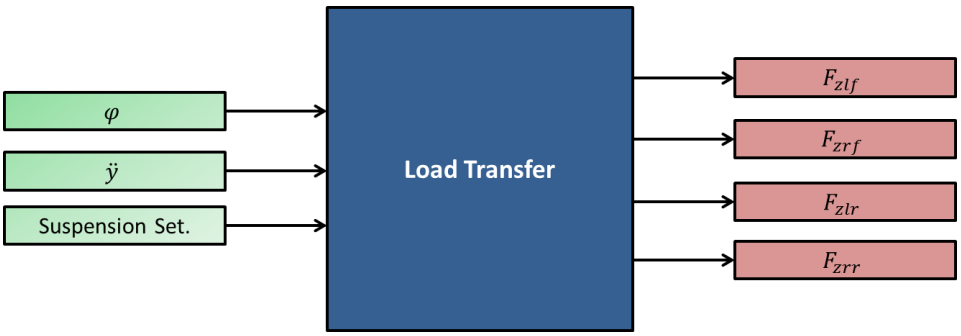

Figure 4-10: Load Transfer

Due to lateral movement of the vehicle, load transfer causes different vertical loads on the four tyres. To calculate the vertical load at each tyre the vehicle lateral acceleration and roll angle is required.

The CG of the vehicle, as estimated by Uys et al. (2006b), does not lie on the centre line of the vehicle but has a slight off-set and can be written as in Equation 4.12 and 4.13 for the effect it has on the left and the right vertical forces of the vehicle, respectively.

$$CG_l = \frac{d_f}{2} + CG_{yoff} \tag{4.12}$$

$$CG_r = \frac{d_f}{2} - CG_{yoff} \tag{4.13}$$

The lateral position of the CG changes due to the roll angle of the vehicle and is calculated as in Equation 4.14 and 4.15 for the effect it has on the front and rear of the vehicle (due to different roll centre heights), respectively.

$$\Delta CG_f = h_f \varphi \tag{4.14}$$

$$\Delta CG_r = h_r \varphi \tag{4.15}$$

The load change due to the roll angle for the four different tyres is calculated as in Equation 4.16 to 4.19.

$$W_{lf} = \frac{mgl_r(CG_l + \Delta CG_f)}{(l_f + l_r)d_f} \tag{4.16}$$

$$W_{rf} = \frac{mgl_r(CG_r - \Delta CG_f)}{(l_f + l_r)d_f} \tag{4.17}$$

$$W_{lr} = \frac{mgl_f(CG_l + \Delta CG_r)}{(l_f + l_r)d_f} \tag{4.18}$$

$$W_{rr} = \frac{mgl_f(CG_r - \Delta CG_r)}{(l_f + l_r)d_f} \tag{4.19}$$

The suspension roll stiffness (K_{sf}, K_{sr}) is calculated using the non-linear suspension force function. The suspension forces are calculated using the roll angle for the front and the rear of the vehicle in Equation 4.20 and 4.21, respectively (Blundell and Harty, 2004).

$$K_{\varphi f} = \frac{1}{2}K_{sf}s^2 \tag{4.20}$$

$$K_{\varphi r} = \frac{1}{2}K_{sr}s^2 \tag{4.21}$$

The load transfer caused by the lateral acceleration of the vehicle is also taken into account as in Equation 4.22 and 4.23 for the front and the rear of the vehicle, respectively.

$$\Delta F_{zf} = \frac{K_{\varphi f}\varphi + \frac{m_b l_r \ddot{y} h_f}{(l_f + l_r)}}{d_f} \tag{4.22}$$

$$\Delta F_{zr} = \frac{K_{\varphi fr}\varphi + \frac{m_b l_f \ddot{y} h_r}{(l_f + l_r)}}{d_f} \tag{4.23}$$

The vertical force at each tyre is then calculated using Equations 4.24 to 4.27.

$$F_{zlf} = W_{lf} - \Delta F_{zf} \tag{4.24}$$

$$F_{zrf} = W_{rf} + \Delta F_{zf} \tag{4.25}$$

$$F_{zlr} = W_{lr} - \Delta F_{zr} \tag{4.26}$$

$$F_{zrr} = W_{rr} + \Delta F_{zr} \tag{4.27}$$

4.1.5 Suspension Forces

The next states that need to be calculated are the suspension forces. This function requires eight inputs, being the displacement and the velocity of each suspension strut, and solves for the suspension force at each strut as shown in Figure 4-11.

The suspension forces are calculated in two parts namely the spring force and the damper force.

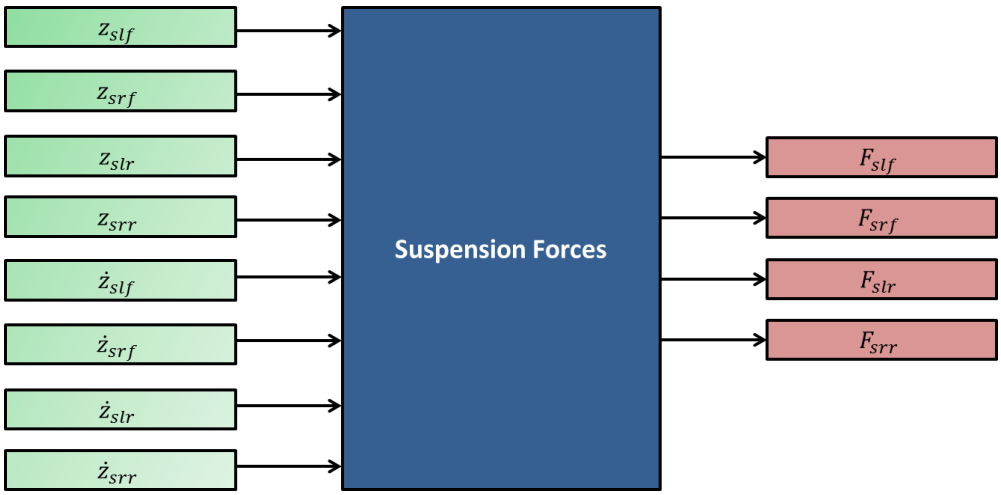

Figure 4-11: Suspension Forces

Spring Force

The force in the spring of the suspension is caused by the compression and expansion of the nitrogen gas in the suspension strut. The force is modelled using the ideal gas law with a gas constant $\gamma = 1.4$ for nitrogen. The gas law is written in Equation 4.28.

$$P_{so} V_{so}^{\gamma} = k \tag{4.28}$$

The piston has a constant area and in the initial position it has a displacement z_{so}, an initial pressure P_{so} and an initial volume V_{so}. The volume above the piston is calculated in Equation 4.29.

$$V_{so} = A z_{so} \tag{4.29}$$

Displacing the piston by z_s results in a change in volume V_{sd} and pressure P_{sd}. This volume is calculated in Equation 4.30.

$$V_{sd} = A(z_{so} + z_s) \tag{4.30}$$

Using the ideal gas law the initial state is compared to the displaced state as in Equation 4.31.

$$P_{so}V_{so}^{\gamma} = P_{sd}V_{sd}^{\gamma} \tag{4.31}$$

The displaced pressure is calculated in Equation 4.32.

$$P_{sd} = P_{so}\left(\frac{V_{so}}{V_{sd}}\right)^{\gamma} \tag{4.32}$$

The relationship between the force and the pressure is written in Equation 4.33.

$$P_{sd} = \frac{F_{sd}}{A} \tag{4.33}$$

The area of the piston remains constant and the spring force generated by the displacement is calculated in Equation 4.35 using Equation 4.34.

$$P_{sd}A = P_{so}A\left(\frac{V_{so}}{V_{sd}}\right)^{\gamma} \tag{4.34}$$

$$F_{sd} = F_{so}\left(\frac{V_{so}}{V_{sd}}\right)^{\gamma} = F_{so}\left(\frac{V_{so}}{A(z_{so} + z_s)}\right)^{\gamma} \tag{4.35}$$

The front suspension has a static force of $3337N$, the rear suspension has a static force of $4392N$ and the piston has a radius of $25mm$. When the $4S_4$ is in the ride comfort mode the accumulator has a static gas volume of $0.5l$ and for the handling mode $0.1l$.

Damping Force

The damping forces are modelled using a four piece-wise continuous quadratic approximation as implemented by Thoresson (2007). The damper fits are defined in Equation 4.36 to Equation 4.39 where $susp_d = 2$ for the hard damper setting and $susp_d = 0.25$ for the soft damper setting.

$$fit_1 = -2000\dot{z}_s^2 + 5000susp_d^{0.9}\dot{z}_s - 100susp_d - 700 \tag{4.36}$$

$$fit_2 = 2(-25000\dot{z}_s^2 + 7000\dot{z}_s) \tag{4.37}$$

$$fit_3 = 40000\dot{z}_s^2 + 10000susp_d^{0.3}\dot{z}_s \tag{4.38}$$

$$fit_4 = 5000(\dot{z}_s - 0.05)^2 + 7000susp_d^{1.3}(\dot{z}_s - 0.05) + 200susp_d + 700 \tag{4.39}$$

The damping force F_{damp} can then be calculated. If the velocity is smaller than zero, then the larger value of fit_1 and fit_2 is used, if the velocity is equal to zero there is no damping and if the velocity is larger than zero, then the smaller value of fit_3 and fit_4 is used. The four different fits are plotted together in Figure 4-12.

The suspension force at each strut is then calculated as the sum of the spring and damper force in Equation 4.40. Only one force is shown, but all four suspension strut forces $(F_{slf}, F_{srf}, F_{slr}, F_{srr})$ are calculated using Equation 4.40.

$$F_{slf} = F_{sd} + F_{damp} \tag{4.40}$$

The sum of the suspension forces on the left and the right of the vehicle is then calculated in Equation 4.41 and 4.42, respectively.

$$F_{Sl} = F_{slf} + F_{slr} \tag{4.41}$$

$$F_{Sr} = F_{srf} + F_{srr} \tag{4.42}$$

4.1.6 Suspension Motion

The front and rear suspension of the Land Rover Defender consists of a solid axle connected to the chassis via two leading and trailing arms, respectively. The suspension motion function assumes that the front and rear roll angles are equal. Figure 4-13 shows the front and rear measured roll angles of the vehicle during a DLC.

A further assumption is made that the suspension struts on the right and left side of the vehicle have the same displacement at the front and at the rear. Figure 4-14 shows a comparrison between the front and rear suspension displacements for the left and the right of the vehicle.

Also the displacement at the left and the right of the vehicle is equal in magnitude but opposite in sign. Figure 4-15 shows a comparrison between the left suspension displacement and the negative value of the right suspension displacement for the front and the rear of the vehicle.

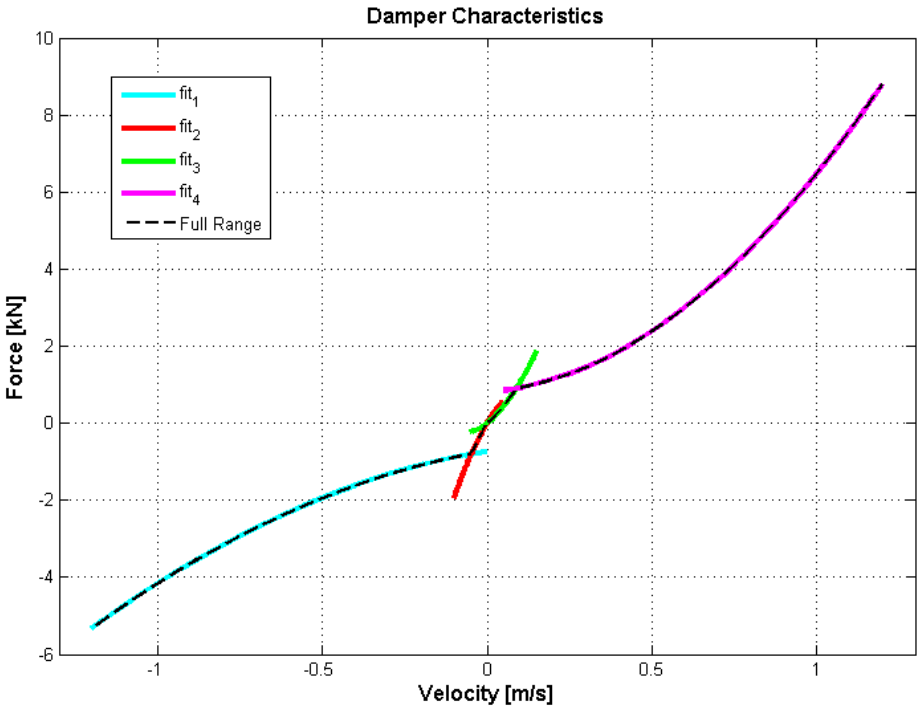

Figure 4-12: Damper Characteristics

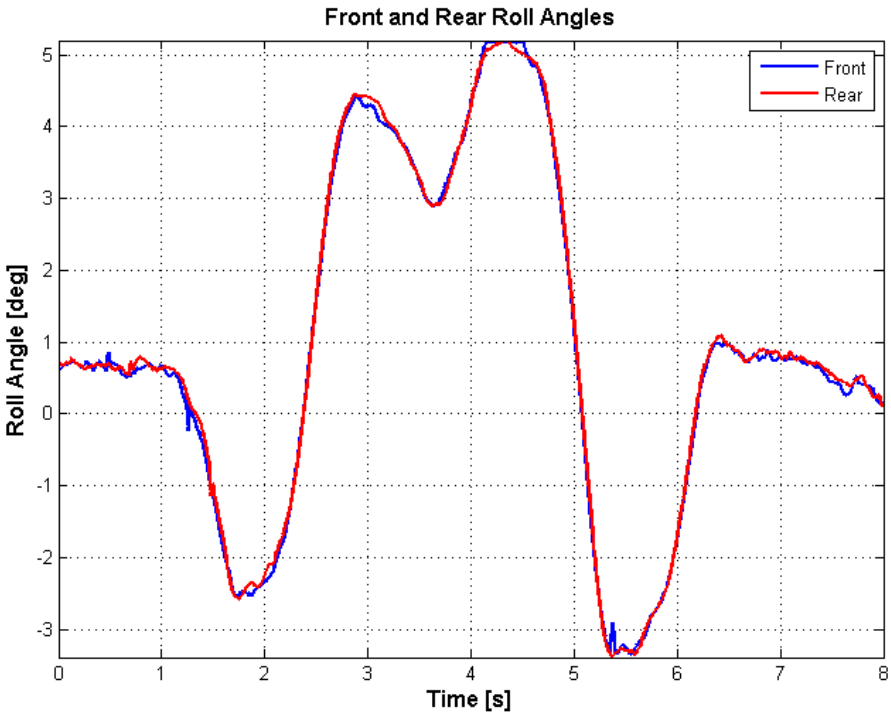

Figure 4-13: Front and rear vehicle roll angles

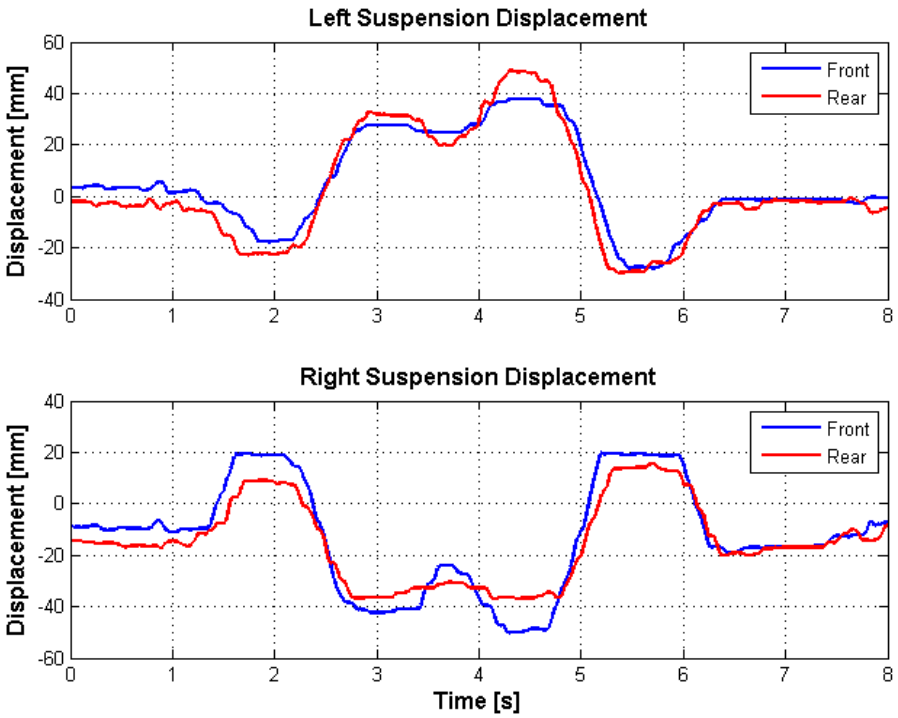

Figure 4-14: Front and rear suspension displacements

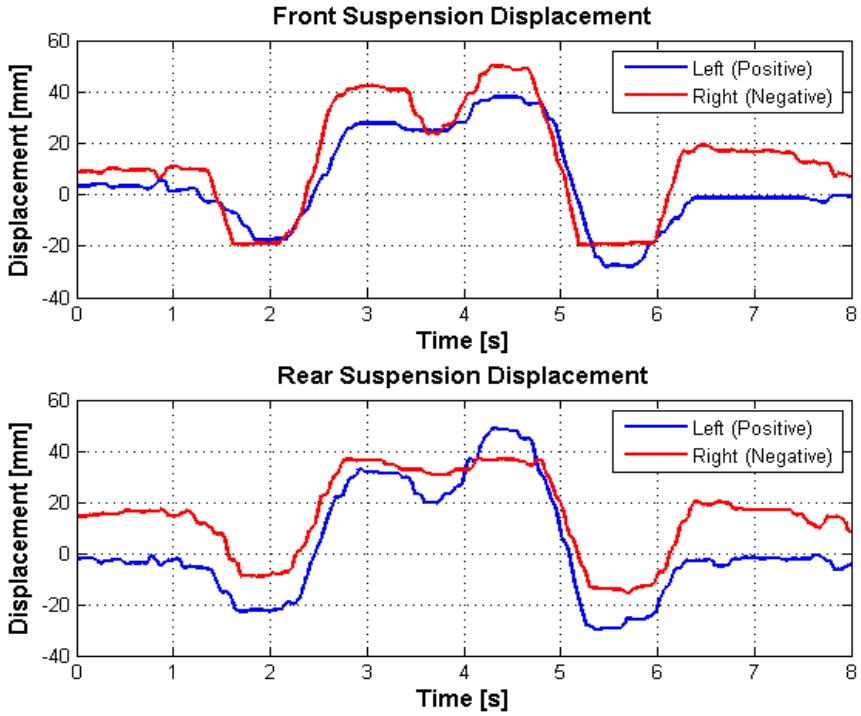

Figure 4-15: Left and right suspension displacement comparison

Figure 4-16 shows the required inputs and the outputs achieved by the function. By assuming small angles, the suspension displacement and suspension velocity is calculated using Equations 4.43

to 4.50. The suspension displacement and velocity is estimated using the geometry of the vehicle and the measured roll angle and roll rate, respectively.

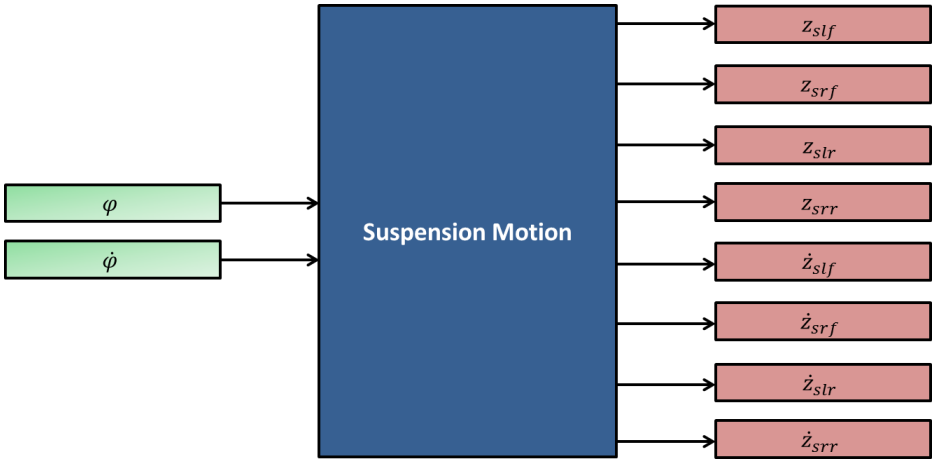

Figure 4-16: Suspension Motion

$$z_{slf} = \frac{-t_s}{2}\varphi \tag{4.43}$$

$$\dot{z}_{slf} = \frac{-t_s}{2}\dot{\varphi} \tag{4.44}$$

$$z_{slr} = z_{slf} \tag{4.45}$$

$$\dot{z}_{slr} = \dot{z}_{slf} \tag{4.46}$$

$$z_{srf} = -z_{slf} \tag{4.47}$$

$$\dot{z}_{srf} = -\dot{z}_{slf} \tag{4.48}$$

$$z_{srr} = -z_{slf} \tag{4.49}$$

$$\dot{z}_{srr} = -\dot{z}_{slf} \tag{4.50}$$

Figure 4-17 shows a comparison between the measured and estimated suspension displacements for the vehicle during a DLC.

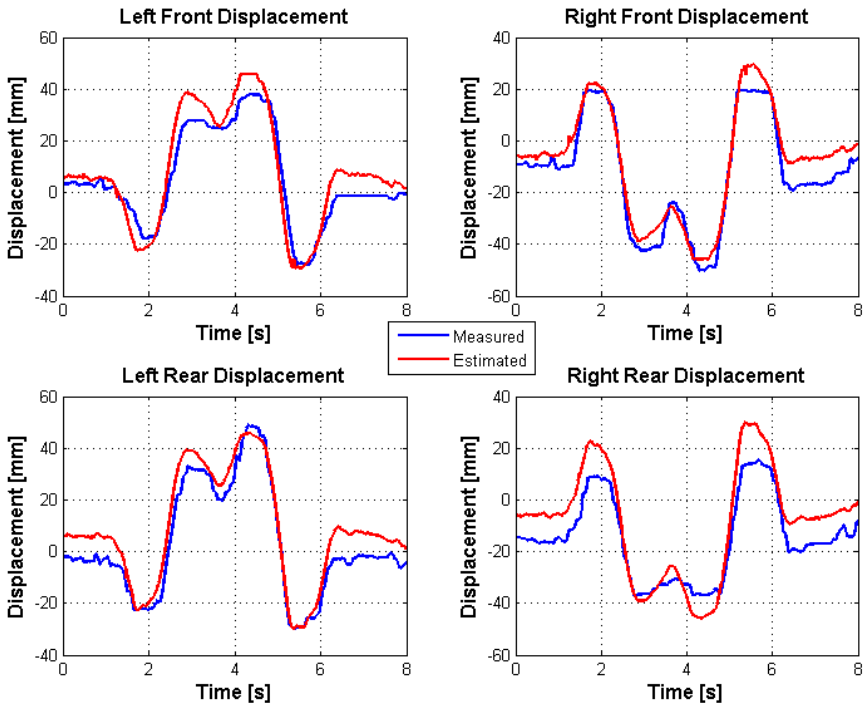

Figure 4-17: Measured suspension displacement vs. estimated suspension displacement

4.1.7 Runge-Kutta Solver

The Runge-Kutta method used by the VPM is written in Equation 4.51 and solves incrementally with a time step h until the required preview time τ has been reached. It means that the model solves for steps $n = 0,1,\ldots\left(\frac{\tau}{h} - 2\right)$. The initial conditions $\left(X_n = \begin{bmatrix}\beta \\ r \\ \dot{\varphi} \\ \varphi\end{bmatrix}\right)$ are measured and the differential equations $f(t_n, X_n)$ are used as the rate at which X_n changes.

$$X_{n+1} = X_n + \frac{1}{6}(k_1 + 2k_2 + 2k_3 + k_4) \tag{4.51}$$

Where

$$k_1 = hf(t_n, X_n) \tag{4.52}$$

$$k_2 = hf\left(t_n + \frac{h}{2}, X_n + \frac{k_1}{2}\right) \tag{4.53}$$

$$k_3 = hf\left(t_n + \frac{h}{2}, X_n + \frac{k_2}{2}\right) \tag{4.54}$$

$$k_4 = hf(t_n + h, X_n + k_3) \tag{4.55}$$

When solving the differential equations all of the current vehicle states at n are used except for the steer angle. Instead the predicted steer angle δ_{n+1} is used as calculated in Equation 4.56, consistent with the initial assumption that the steer rate remains constant for the entire preview time.

$$\delta_{n+1} = \delta_n + \dot{\delta} h \tag{4.56}$$

For the first Runge-Kutta iteration $(n = 0)$ the initial inputs are used with the predicted steer angle (δ_1) while for step $n = 1,2, \ldots \left(\frac{\tau}{h} - 2\right)$ the Runge-Kutta outputs are used as the Runge-Kutta inputs, except for the final step where the solution is used as a final VPM output as shown in Figure 4-18.

The first differential equation, which defines the rate at which the side-slip angle changes, can be written as seen in Equation 4.57 by rearranging Equation 4.1.

$$\dot{\beta} = \frac{\left(F_{lf} + F_{rf} + F_{lr} + F_{rr}\right)}{mV} - r \tag{4.57}$$

The second differential equation can be written as in Equation 4.58 by rearranging Equation 4.2. Equation 4.58 then becomes the equation that defines the rate at which the yaw rate changes.

$$\dot{r} = \frac{l_f\left(F_{lf} + F_{rf}\right) - l_r(F_{lr} + F_{rr})}{I_z} \tag{4.58}$$

The third differential equation, which defines the rate at which the roll rate changes, is written as in Equation 4.59 which is a rearrangement of Equation 4.3. The final differential equation is the rate at which the roll angle changes which is simply the roll rate and can be written as in Equation 4.60.

$$\ddot{\varphi} = \frac{(F_{Sl} - F_{Sr})\frac{t_s}{2} + h_{cg}\left(F_{yl} + F_{yr}\right)}{I_x} \tag{4.59}$$

$$\dot{\varphi} = \dot{\varphi} \tag{4.60}$$

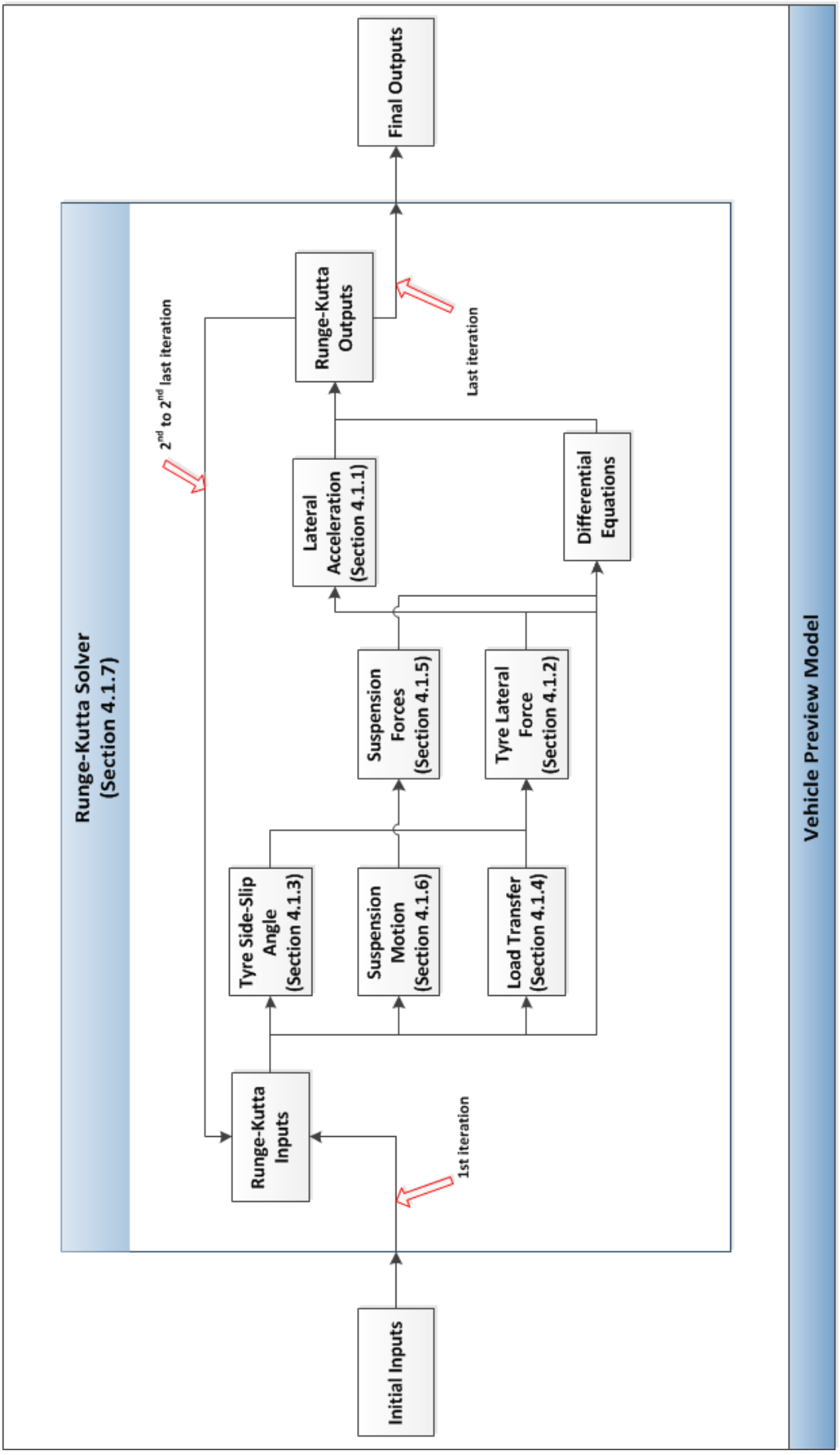

Figure 4-18: Vehicle Preview Model Schematic

4.2 VPM Validation

It is important for the VPM to be validated before it gets implemented on the vehicle for real-time predictions. It is firstly validated using ADAMS simulations and then validated using experimentally obtained data.

4.2.1 VPM results using simulation data as input

To validate the VPM, simulations are run using the validated ADAMS vehicle model. Figure 4-19 and Figure 4-20 shows a comparison between the simulated (plotted with a solid red) and predicted (plotted with a dotted blue) results for the vehicle performing a DLC at 60 km/h with preview times of 50 and 200 ms, respectively. Figure 4-21 and Figure 4-22 shows a comparison between the simulated and predicted for the vehicle following a sinusoidal path with increasing frequency with preview times of 50 and 200 ms, respectively.

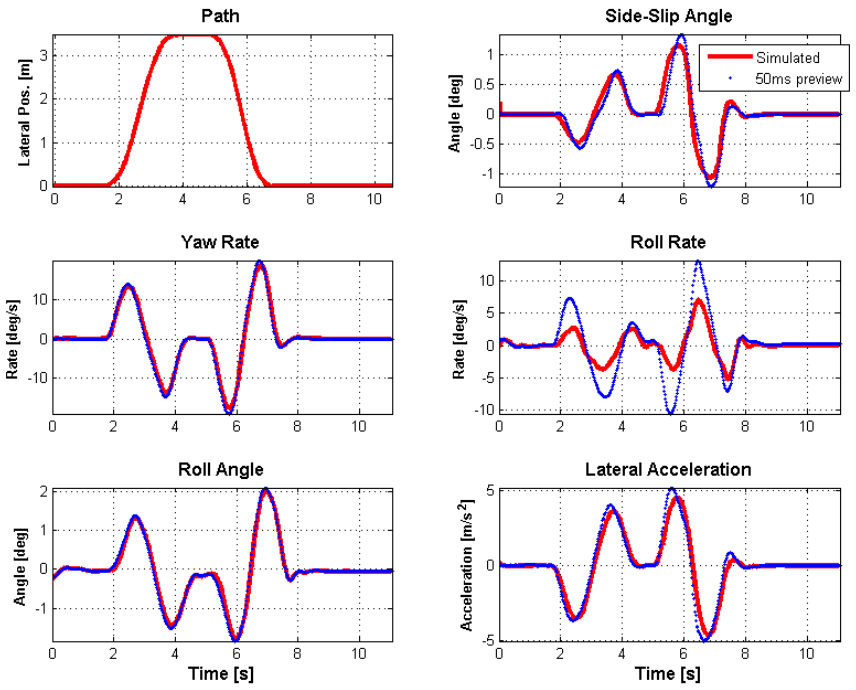

Figure 4-19: Simulation based preview model validation for DLC at 60 km/h with 50 ms preview

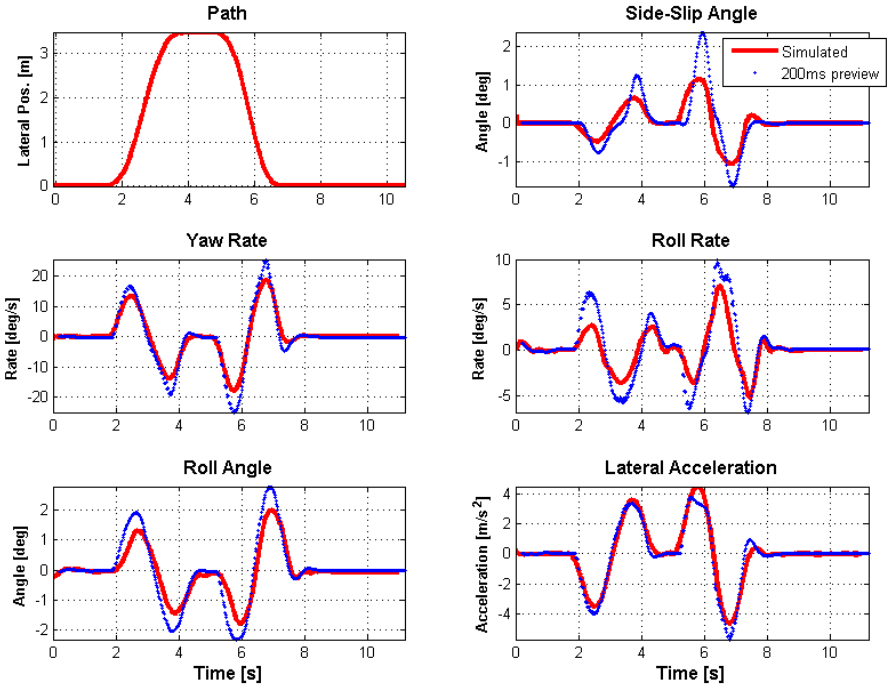

Figure 4-20: Simulation based preview model validation for DLC at 60 km/h with 200 ms preview

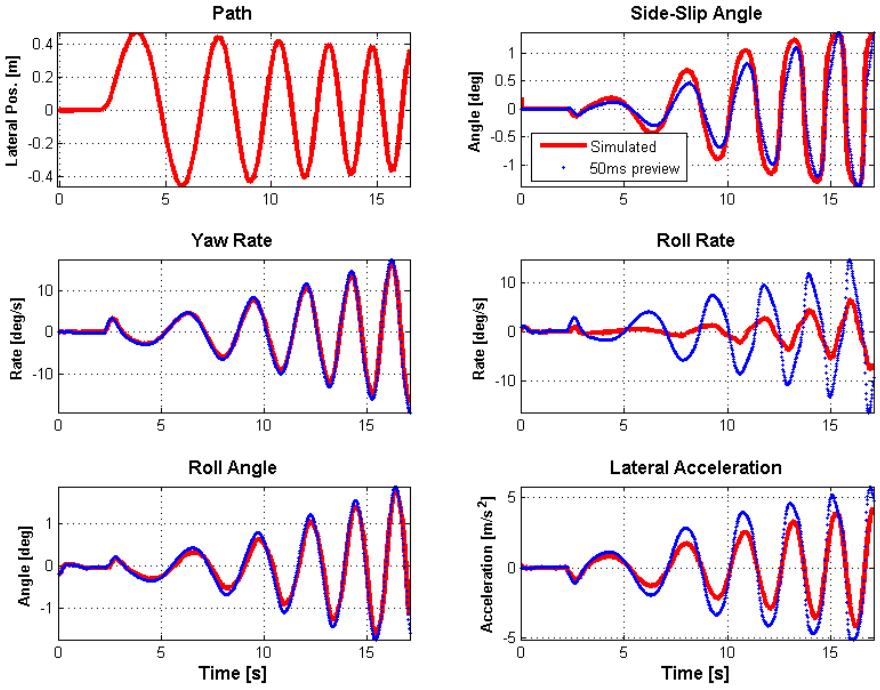

Figure 4-21: Simulation based preview model validation for sinusoidal road at 60 km/h with 50 ms preview

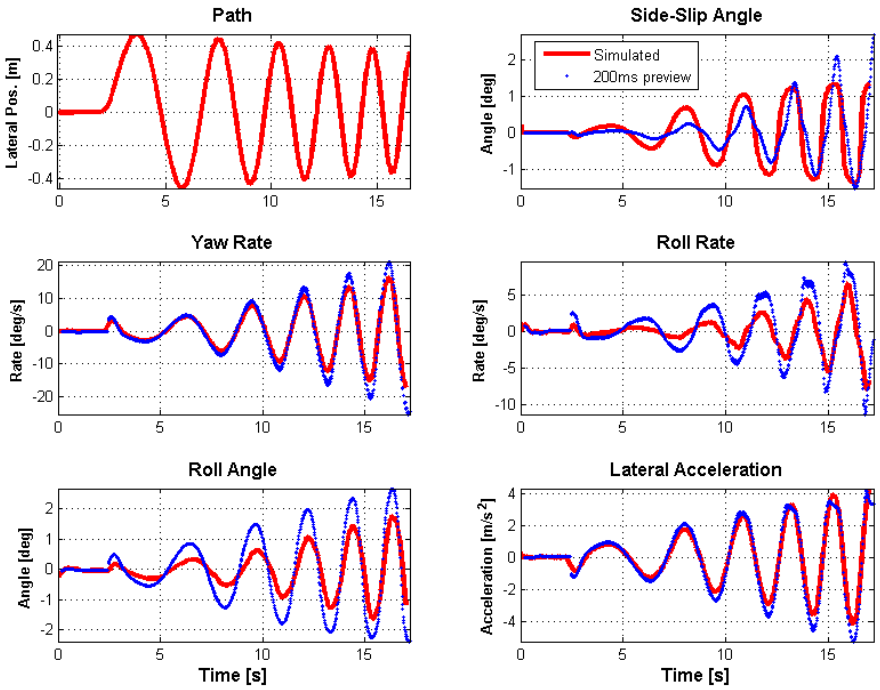

Figure 4-22: Simulation based preview model validation for sinusoidal road at 60 km/h with 200 ms preview

It is clear from these figures that the measured and the predicted states correspond well. It can also be seen that the accuracy of the different predicted states differ when using different preview times. In Figure 4-19 and Figure 4-21, with a preview time of 50 ms, it is clear that the roll angle is more accurate than the lateral acceleration and in Figure 4-20 and Figure 4-22, with a preview time of 200 ms, the lateral acceleration is more accurate than the roll angle. This will be investigated in more detail later.

From the above results it can be seen that the VPM works well when using ADAMS simulation data as input.

4.2.2 VPM results using experimental data as input

The following figures show the results of using experimentally obtained data as input to the VPM. Figure 4-23 and Figure 4-24 shows the results of the vehicle performing a DLC at 71 km/h with a preview time of 50 and 200 ms respectively. Figure 4-25 and Figure 4-26 shows the results of the vehicle attempting to follow a sinusoidal path at 55 km/h with preview times of 50 and 200 ms respectively.

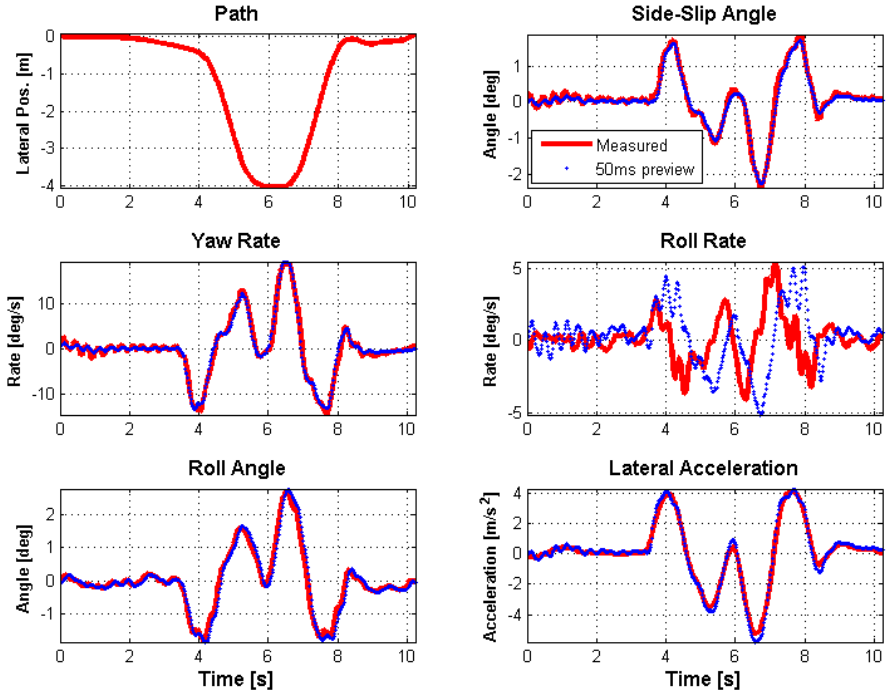

Figure 4-23: Experimental preview model validation for DLC at 71 km/h with 50 ms preview

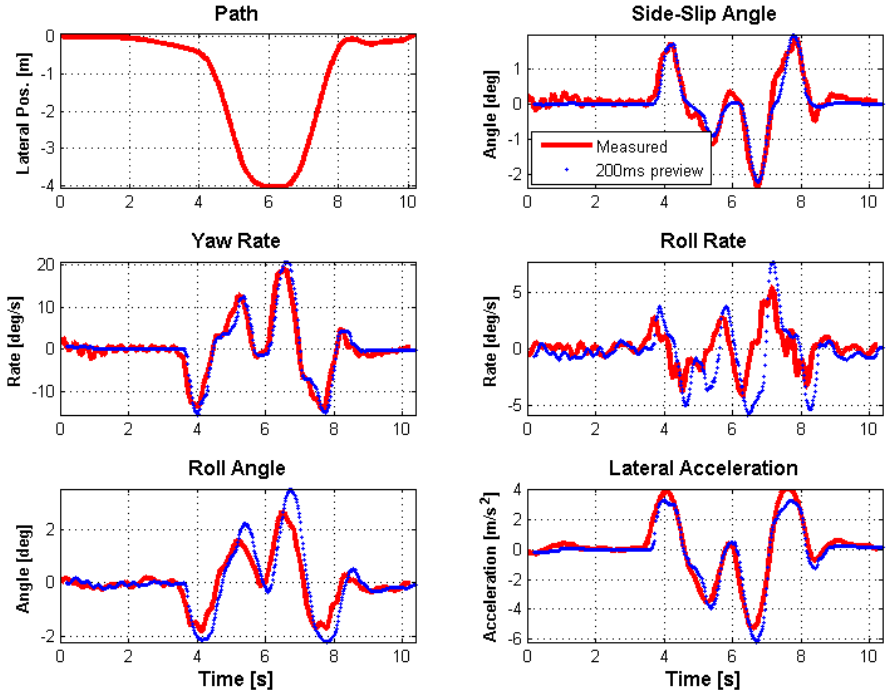

Figure 4-24: Experimental preview model validation for DLC at 71 km/h with 200 ms preview

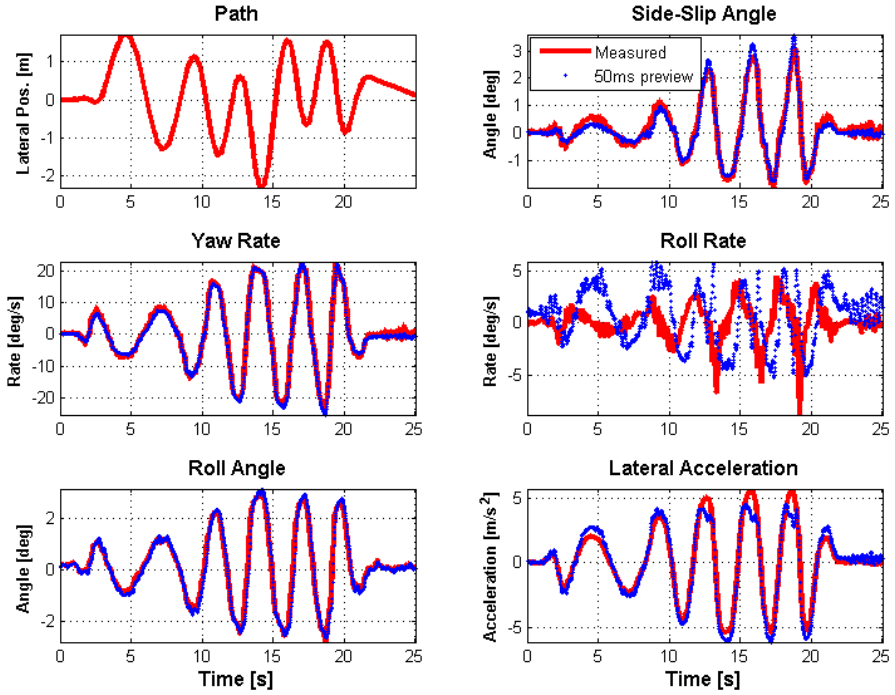

Figure 4-25: Experimental preview model validation for sinusoidal road at 55 km/h with 50 ms preview

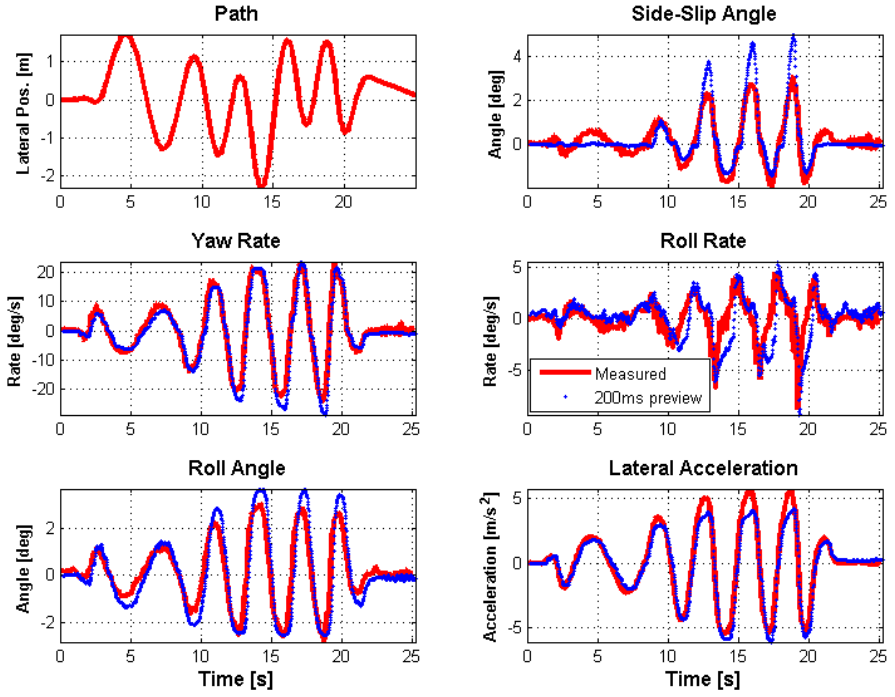

Figure 4-26: Experimental preview model validation for sinusoidal road at 55 km/h with 200 ms preview

As with the simulation results before; the accuracy of the different states differs depending on the preview time. It seems like the predicted lateral acceleration is more accurate at 200 ms than it is at $50ms$ and once again all states are predicted accurately except for the roll rate. The accuracy of the VPM at different preview times will now be investigated.

4.2.3 Preview Time Accuracy

The accuracy of the VPM at different preview times is investigated by using the R^2. Also the effect of using different solving time steps is taken into account. Figure 4-27 shows the R^2 for the different predicted vehicle states as a function of preview time. As seen before the preview accuracy for the different states vary depending on the preview time.

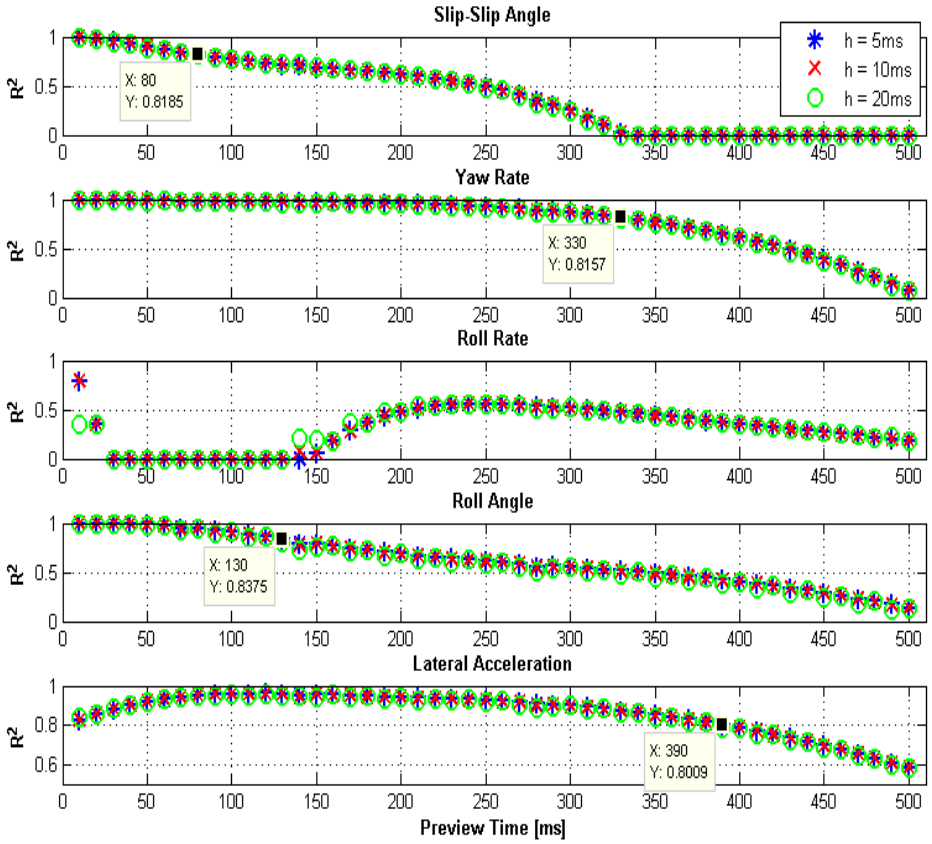

Figure 4-27: Coefficient of Determination for Predicted States

By assuming that a R^2 value greater than 0.9 represents excellent correlation and that an acceptable R^2 value lies above 0.8, the corresponding preview times for the different states are tabulated in Table 4-1.

Table 4-1: Acceptable preview times based on R^2

Parameter	Preview time where $R^2 > 0.9$	Preview time where $R^2 > 0.8$
Side-Slip Angle	50	80
Yaw Rate	270	330
Roll Rate	None	None
Roll Angle	100	130
Lateral Acceleration	300	390

The side-slip angle of the vehicle is accurately predicted up to a preview time of $80ms$ and this could possibly be improved by improving the tyre force estimation of the VPM.

The worst preview accuracy is that of the roll rate. This is because the calculated suspension forces do not include any suspension friction. By improving the suspension model, the roll rate and the roll angle predictions can be improved. The yaw rate and lateral acceleration can be accurately predicted by up to 330 and 390 ms, respectively.

The VPM was successfully developed and validated using simulations and experimentally obtained data. The next step is to implemented the VPM to the test vehicle in real-time.

5 IMPLEMENTATION OF THE VPM ON THE VEHICLE

After successful validation of the VPM, by means of simulations and experimentally obtained data, the VPM is implemented on the vehicle to solve real-time. The VPM is coded in C++ and implemented on an embedded PC, with a Linux operating system, that is mounted in the vehicle.

All the vehicle sensors use the analog to digital converters as inputs to the PC-104, as shown in Figure 5-1. The PC-104 then solves the VPM and uses an analog output to send the predicted lateral acceleration to a second PC-104, as developed by Els (2006), that runs the RRMS strategy. The second PC-104 uses digital outputs to trigger the valves of the $4S_4$ to switch to different suspension modes.

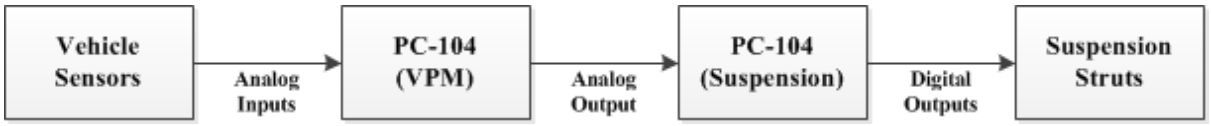

Figure 5-1: Block diagram of control system

In the future it would be possible to run the VPM and RRMS strategy on the same PC-104, but for this study it was better to use two separate computers so that the new strategy could be compared directly to the original unchanged RRMS strategy.

The VPM performance will be analysed and tests will be performed to check whether the RRMS switching delay could be improved.

5.1 Model Performance

The embedded computer is a Helios that consists of a PC-104 single board computer with a Vortex86DX CPU and integrated auto calibrating data acquisition as developed by Diamond Systems (2013). The Vortex86DX CPU is a 800 MHz single core processor with 256 MB of on-board DRAM. It has 16 digital inputs, 16 digital outputs, 16 analog inputs with 16-bit resolution and 4 analog outputs with 12-bit resolution. This system will be referred to as PC-104.

For comparison the VPM performance will also be analysed in C++ using a desktop with 64-bit Windows. The desktop has a 3.2 GHz quad core processor with 16 GB of ram and uses *i*5-3470 architecture and will be referred to as 'PC'.

5.1.1 Model Profile

An embedded profiler is used to analyse the VPM performance and to understand which parts uses the largest percentage of the total time. This is done using the PC-104 as well as the PC for comparison.

Table 5-1 shows all the functions that the VPM uses, how many times each function is called and the percentage of the total time used by each function. The information in Table 5-1 was obtained using a preview time of 200 ms and a solving time-step of 10 ms. The number of calls of each function is dependent on both of these parameters, but the percentage time used stays the same relative to each other.

Table 5-1: Model Performance

Function	Number of Calls	Percentage of Total Time (PC-104)	Percentage of Total Time (PC)
Interpolation	80	1%	1%
Load Transfer	80	4%	5%
Tyre Forces	320	32%	18%
Suspension Forces Front	320	28%	33%
Suspension Forces Rear	320	28%	31%
Differential Equations	80	7%	12%

The interpolation, load transfer and tyre force functions uses 1%, 4% and 32% of the total time to solve on the PC-104, respectively. The tyre lateral force is estimated using the Magic Formula, as discussed before, which uses sine and arctangent trigonometric functions. The solving times for these trigonometric functions on the PC-104 are slow when compared to the solving times when using the PC. The suspension force functions (front and rear) are called a total of 640 times and takes 56% of the total time to solve, making it the most time costly function. The differential equations makes up 7% of the total time.

5.1.2 Model Solving Time

Using the PC-104 in the vehicle, the solving time of the VPM is measured for different preview times and time steps. The solving time is an important aspect that needs to be investigated.

Els (2006) decided to use a sampling frequency of 100 Hz for the RRMS strategy, so it was decided to use the same sampling frequency for the VPM for an accurate comparison. Further investigation should be done to determine the minimum required sampling frequency. Using a smaller sampling frequency would allow the model to solve for longer preview times.

If the VPM takes longer to solve than the sampling frequency of 100 Hz (ie. 10 ms loop time), overflows will cause interrupts to be missed. Table 5-2 shows the average solving time for different preview times and solving time steps.

It can be seen from Table 5-2 that the solving frequency is higher than the sampling frequency for most of the cases except for a preview time of 200 and 300 ms with a time step of 5 and 300 ms with

a time step of 10 ms. This means that when the VPM has a preview time of 200 ms a time step of 10 or 20 ms should be used and for 300 ms a time step of 20 ms should be used.

For a preview time of 200 ms, with a solving time step of 10 ms, the VPM takes 7.63 ms to solve on the PC-104 and 0.23 ms to solve on the PC. It means that the solving time of the VPM when using the more powerful PC is about 33 times faster. This comparison is used to show that the solving time problem is relative to the computer power available and if the VPM is solved on a more powerful processor, faster solving times and longer preview times can be achieved.

Table 5-2: Model solving time for different preview times and time steps.

Preview Time [ms]	Time Step [ms]	Solving Time [ms]	Solving Frequency [Hz]
50	5	3.84	260.42
	10	1.91	523.56
	20	0.79	1265.82
100	5	7.67	130.38
	10	3.84	260.42
	20	1.96	510.20
200	5	15.26	**65.53**
	10	7.63	131.06
	20	3.84	260.42
300	5	22.81	**43.84**
	10	11.44	**87.41**
	20	5.80	172.41

5.2 Implementing the VPM to improve the RRMS strategy

This paragraph investigates whether the problems associated with the time delay of the RRMS strategy can be improved by using the predicted lateral acceleration instead of the measured lateral acceleration. The lateral acceleration preview accuracy will be considered when making decisions on the real-time implementation of the VPM.

The original RRMS strategy is compared to the RRMS strategy combined with the VPM by performing numerous DLCs. Figure 5-2 shows the results of a DLC performed using the original RRMS strategy and the RRMS strategy combined with the VPM.

The vehicle path is plotted in black in Figure 5-2.a combined with the suspension switching for both strategies. The blue line shows the suspension switching for the original RRMS method and the red line for the RRMS method combined with the VPM.

The measured lateral acceleration during the DLC for the RRMS method is plotted in blue in Figure 5-2.b and the predicted lateral acceleration for the RRMS method combined with the VPM is plotted in green. Figure 5-2.c shows the roll angles for the two different methods.

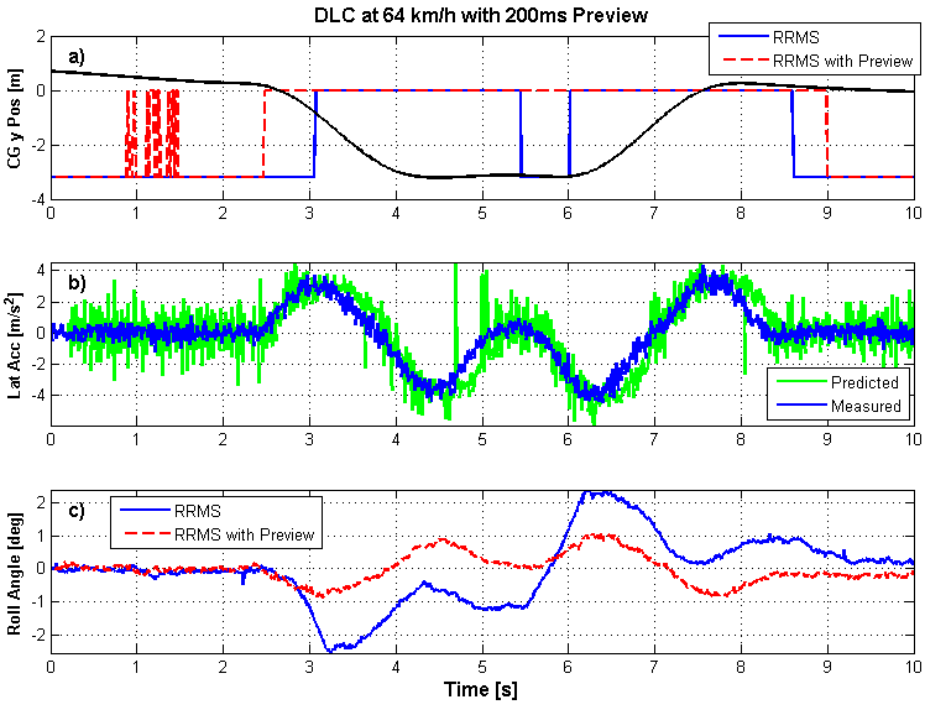

Figure 5-2: DLC comparison of switching methods at 60km/h with 200ms preview

The RRMS method combined with the VPM switches to the hard suspension earlier than the original RRMS method. Using the predicted lateral acceleration (instead of the measured) with the RRMS method yields an improvement of 42% in the RMS value of the roll angle and a 43% improvement in the maximum roll angle.

Even though this is a major improvement compared to the original RRMS strategy, it might not be a fair comparison. It is also clear from Figure 5-2.b that the predicted lateral acceleration is noisier than the measured acceleration. In this case, the VPM makes the RRMS strategy more sensitive and causes spurious switching of the suspension. Around 1 second it can be seen that the vehicle is driving in a straight line, which means the lateral acceleration should be close to zero as with the measured results, but this is clearly not the case with the predicted lateral acceleration. The predicted lateral acceleration is jumping between positive and negative 3 m/s^2 causing spurious switching of the suspension as indicated in Figure 5-2.a (red line).

Using post processing of the data and filtering different inputs, it was found that the steer rate is the cause of this problem. The steer rate is calculated in the model by differentiating two consecutive steer angle values as in Equation 5.1.

$$\dot{\delta}(i) = \frac{\delta(i) - \delta(i-1)}{t(i) - t(i-1)} \tag{5.1}$$

As discussed before, the VPM uses the current steer angle and steer rate and by the assumption that the steer rate remains constant for the entire preview time, predicts the future vehicle state.

To better understand the effect that this method of differentiating has on the steer rate values, the measured steer angle and calculated steer rate values are shown in Figure 5-3. It is clear that the steer angle measurements have little noise, but after differentiating the steer angle to get the steer rate, the noise is significantly amplified.

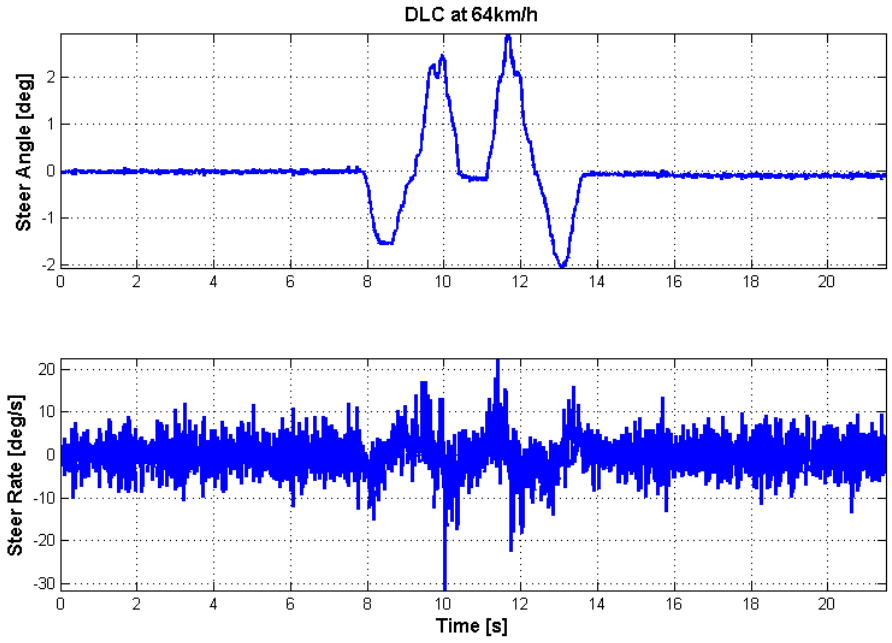

Figure 5-3: Steer angle and steer rate during DLC

Figure 5-4 shows a comparison between the original predicted values and predicted values using a filtered steer rate. The steer rate is passed through a 2.5 Hz low-pass filter. Figure 5-4.a shows the original steer rate plotted in red and the filtered steer rate plotted in blue. Figure 5-4.b and Figure 5-4.c shows the originally predicted yaw rate and lateral acceleration in red, the measured yaw rate and lateral acceleration in green and the predicted yaw rate and lateral acceleration achieved when using the filtered steer rate in blue.

It is clear that the steer rate values are the big culprit causing the noisy predictions. Using the filter described above to filter the steer rate data creates further time delays that might compromise the performance of the VPM; therefore, a different type of method to compute a clean steer rate needs to be found.

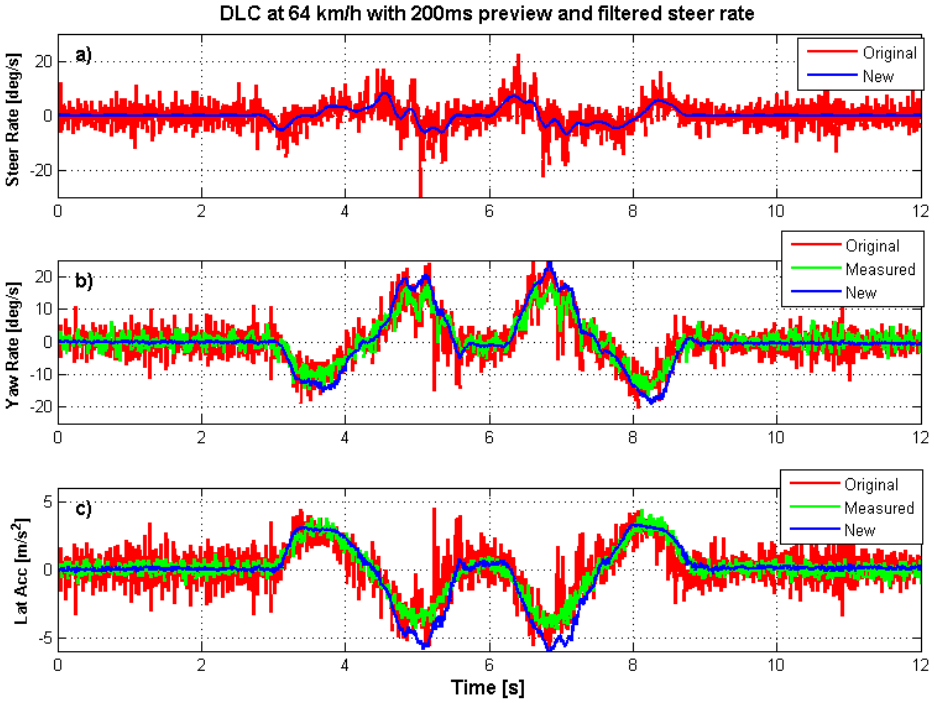

Figure 5-4: DLC comparison of preview results using original and filtered steer rate

5.3 Improving Steer Rate Values

It is clear that the steer rate values play a major role in the accuracy of the VPM and that noisy values cause noisy preview results. Figure 5-5 shows the preview results where the steer rate was set to zero for an entire DLC. The predicted values are less noisy, but it is also clear that this causes a lag in the preview results eliminating the preview.

The VPM uses backward differentiation of two consecutive points to calculate the steer rate. The model runs at 100 Hz which makes the change in time when calculating the steer rate small. The smaller the change in time, the more the noise is amplified. Therefore the steer rate can be calculated by using the backwards differencing method as written in Equation 5.2, which increases the change in time by increasing the spacing between points.

$$\dot{\delta}(i) = \frac{\delta(i) - \delta(i-j)}{t(i) - t(i-j)} \tag{5.2}$$

Where i is the current point and j is the other point being used. This method is similar to a digital filter where all the values between point i and point j are made zero. To investigate the effect of using Equation 5.2, a simple sinusoidal signal with added white noise is differentiated using different

values for j. Figure 5-6.a shows the distance travelled and Figure 5-6.b shows the velocity calculated using different spacing between points for the backward differencing method.

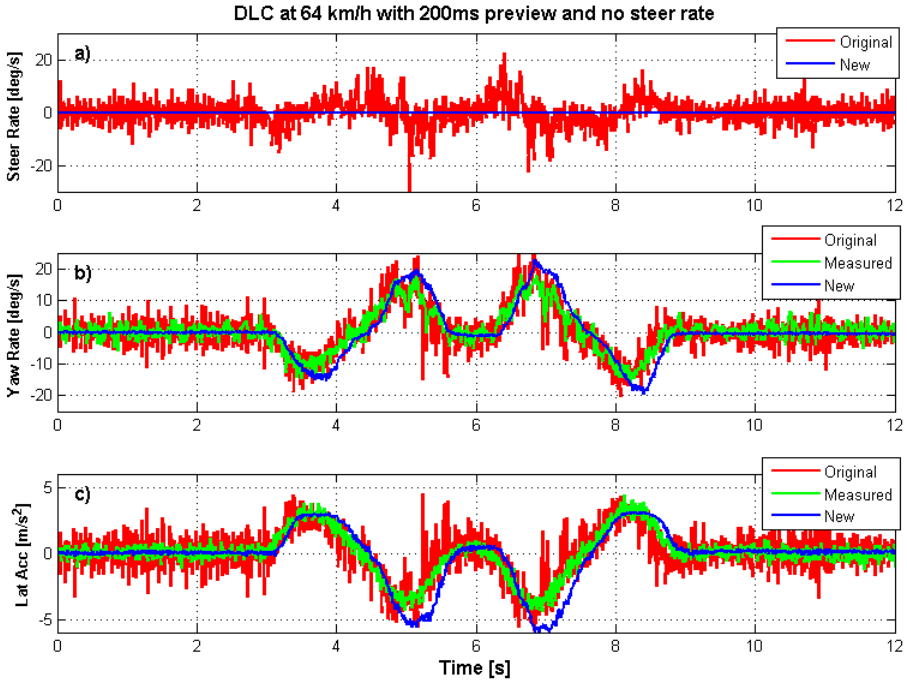

Figure 5-5: DLC preview results at 60km/h with 200ms preview and no steer rate

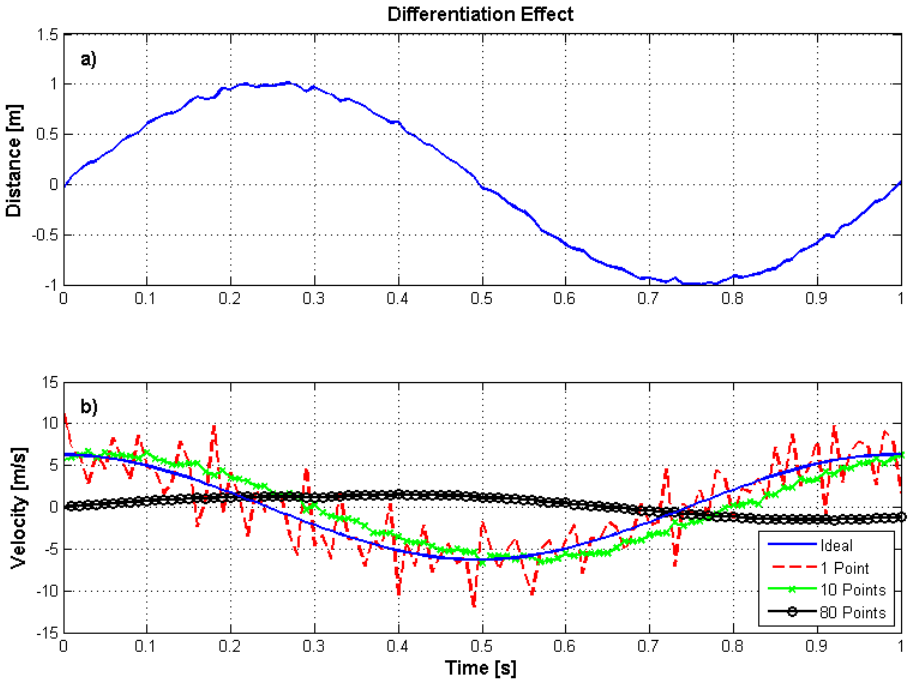

Figure 5-6: Differentiation effect

The solid blue line in Figure 5-6.b shows the ideal velocity of the movement. The red dotted line is the velocity when using two consecutive points ($j = 1$), the green line with a star shows the velocity when using a point spacing of ten ($j = 10$) and the black line with a circle a spacing of 80 ($j = 80$).

When comparing the velocity using one point to the velocity using ten points, it is clear that by increasing the number of points between samples for the backward differencing method that the noise decreases and the lag increases. When the spacing between points gets too large, for example using eighty points, this method yields completely misleading velocities. Therefore it is important to use the optimum spacing between points.

To find the ideal spacing size that needs to be used, experimentally obtained data will be used. The results for using different spacing sizes to calculate the steer rate can be seen in Figure 5-7 for a DLC performed at 64 km/h.

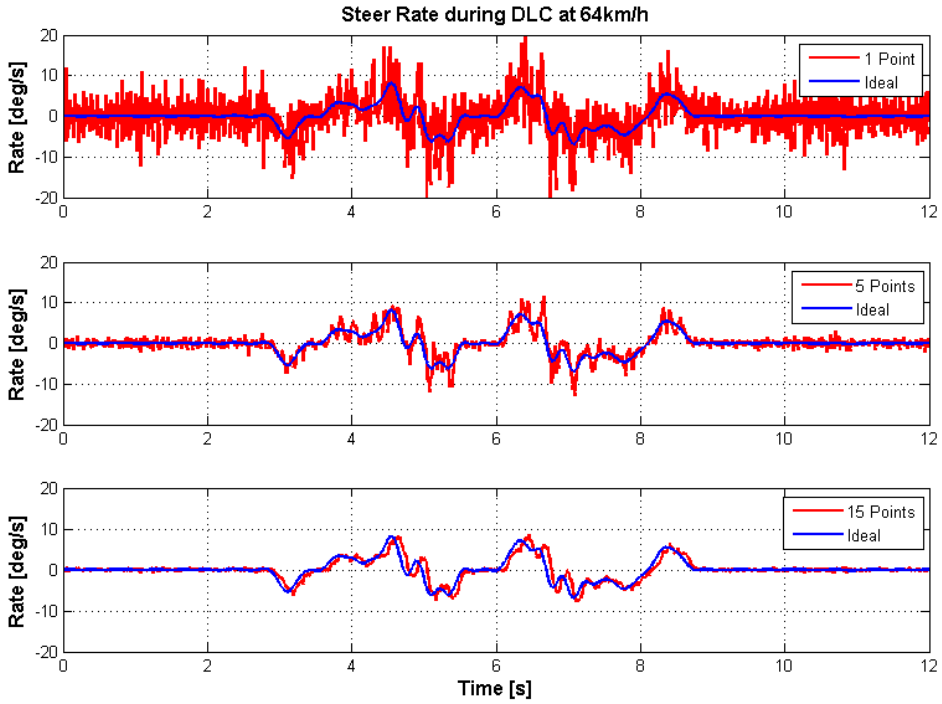

Figure 5-7: Differentiation effect on steer rate during DLC at 60km/h

Once again the noise decreases and the lag increases as the spacing increases. Performing Fast Fourier Transforms (FFTs) on the unfiltered steer angle and steer rate gives us an idea at which frequency the steering happens and the number of points that need to be used can be calculated. Figure 5-8 and Figure 5-9 show the FFT results for the unfiltered steer angle and the unfiltered steer rate, respectively.

The steering inputs have a frequency content up to $f_c = 4.15$ Hz after which the magnitude drops. Following the Nyquist sampling theorem, which states that the sampling frequency (f_d) should be at least twice that of the highest frequency contained (f_c), the required sampling frequency is calculated in Equation 5.3 and Equation 5.4.

$$f_d \geq 2f_c \tag{5.3}$$

$$f_d \geq (2)(4.15) \geq 8.3Hz \tag{5.4}$$

From this theorem we can estimate the largest allowable spacing between two points being differentiated. The sampling frequency of the VPM is $f_s = 100$ Hz which means the time step between points is 0.01 s. The maximum number of points that can be used is calculated in Equation 5.5.

$$n_p \leq \frac{1}{(0.01)(f_d)} = \frac{1}{(0.01)(8.3)} \leq 12 \tag{5.5}$$

This is an estimate of the number of points that need to be used and to find the optimum number of points a sensitivity analysis is performed. Point intervals from one to twenty five were analysed and the different calculated steer rates are compared to the ideal steer rate by calculating the R^2 and RMS error. The results for a DLC at 64 km/h can be seen in Figure 5-10.

Therefore for a DLC performed at 64 km/h the optimum spacing between two steer angle values is 10. The optimum number of points for a DLC at 70 km/h and 80 km/h was also investigated and found to be 10 and 9, respectively.

The FFTs of the steer rate using 10 points and the original method using 1 point are shown in Figure 5-11. It can be seen that after 4.15 Hz the magnitude of the blue FFT drops, as expected.

From the above results it is clear that using a spacing of about 9 or 10 points yields the most accurate steer rate. It is also important to determine the effect that the number of points has on the VPM preview accuracy and not only on the steer rate accuracy. Figure 5-12 shows the predicted values when using backwards differentiation in order to calculate the steering rate with 9 points.

When comparing the measured lateral acceleration to the predicted acceleration, it is clear that the measured acceleration has more noise present. When the RRMS method takes the measured vertical and lateral acceleration values, the noise does not have such a big effect, since the noise is present in both signals. When the RRMS uses the predicted lateral acceleration with the measured vertical acceleration, the fact that the predicted signal is less noisy might cause a problem. The noise in the measured vertical acceleration makes the RRMS method more sensitive to switching, as seen before.

Figure 5-13 shows the FFTs of the measured lateral acceleration in blue and the predicted lateral acceleration in red. The difference in signal energy between the measured and the predicted signals can clearly be seen.

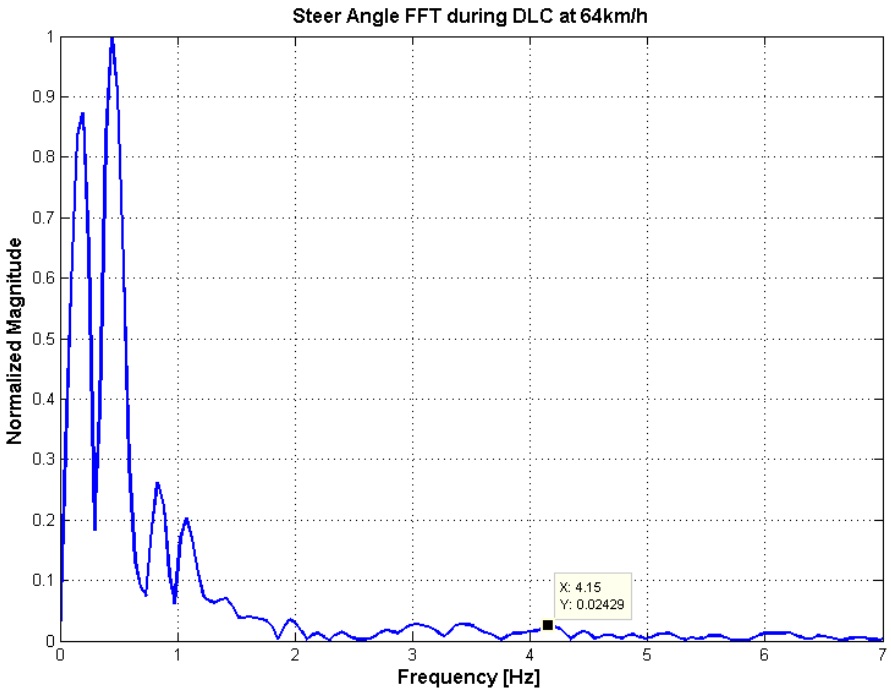

Figure 5-8: Steer angle FFT during DLC at 64km/h

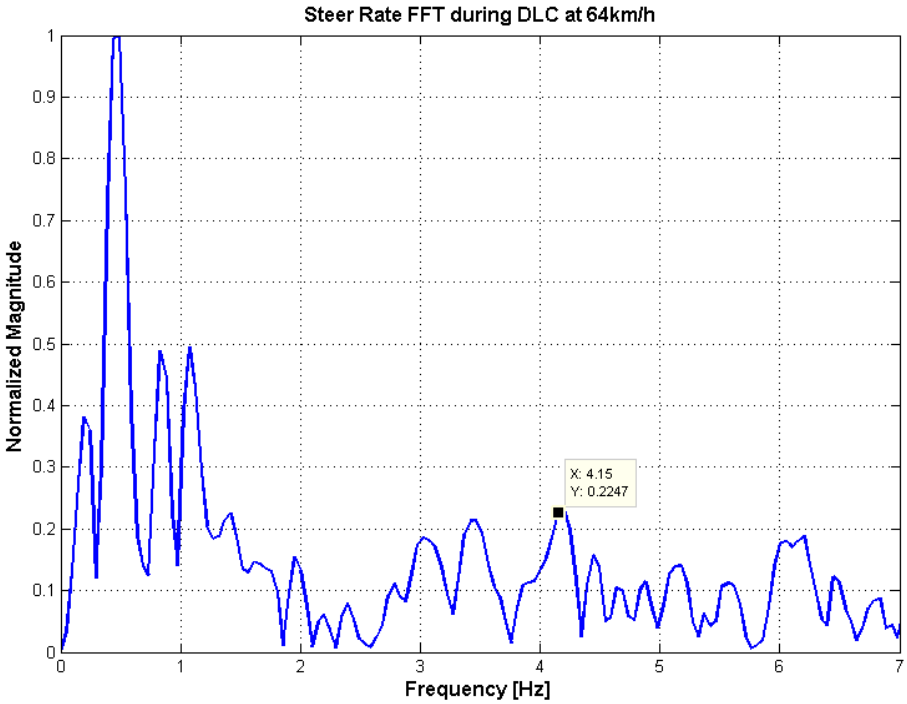

Figure 5-9: Filtered steer rate FFT during DLC at 64km/h

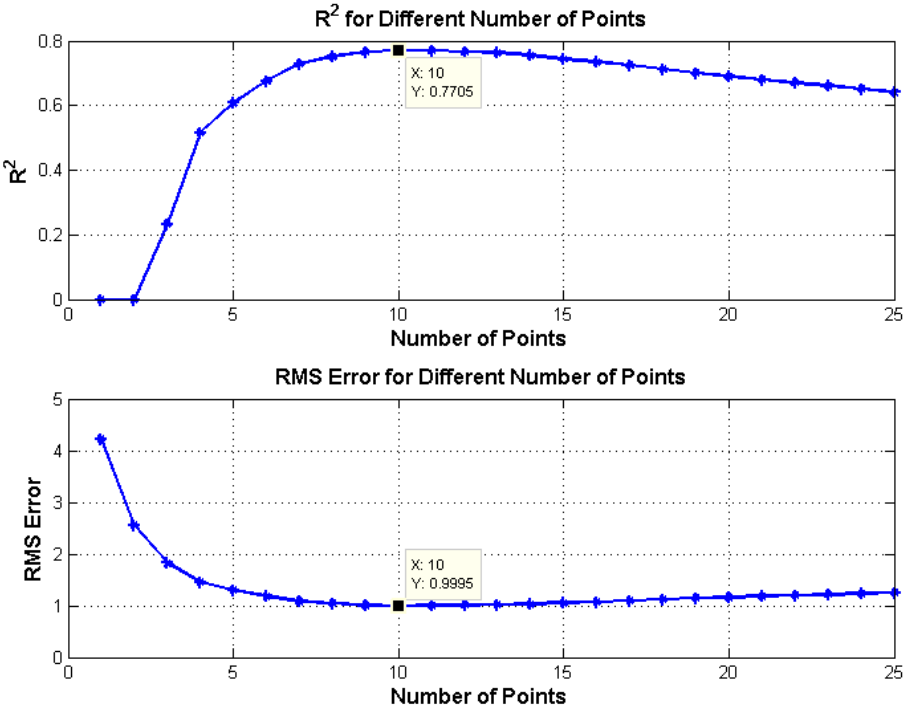

Figure 5-10: Point interval sensitivity during DLC at 64km/h

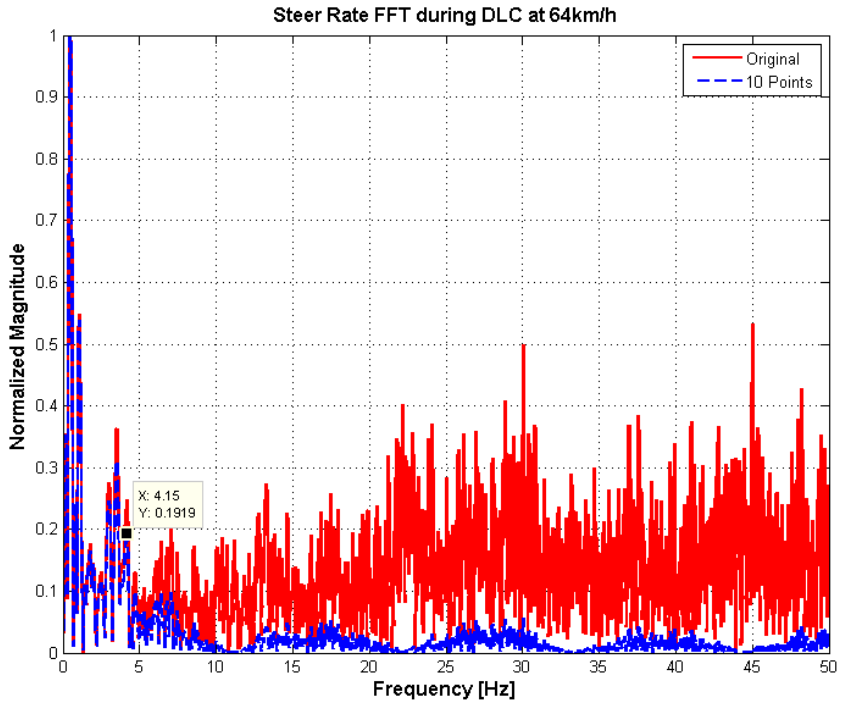

Figure 5-11: Steer rate FFT during DLC at 64km/h using 2 points with 10 point spacing

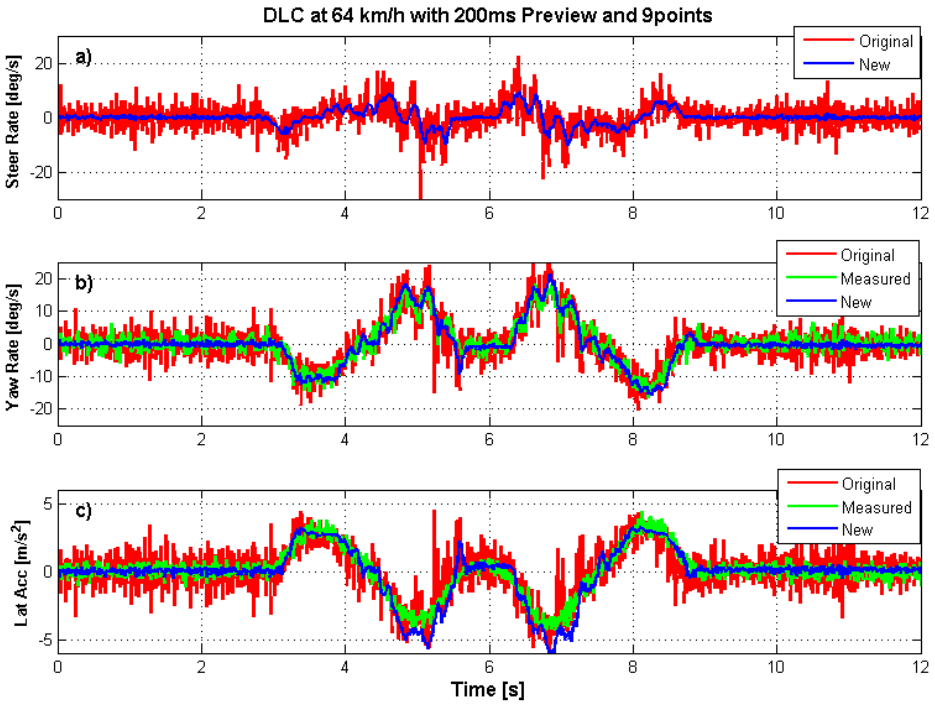

Figure 5-12: DLC at 64km/h using 9 points

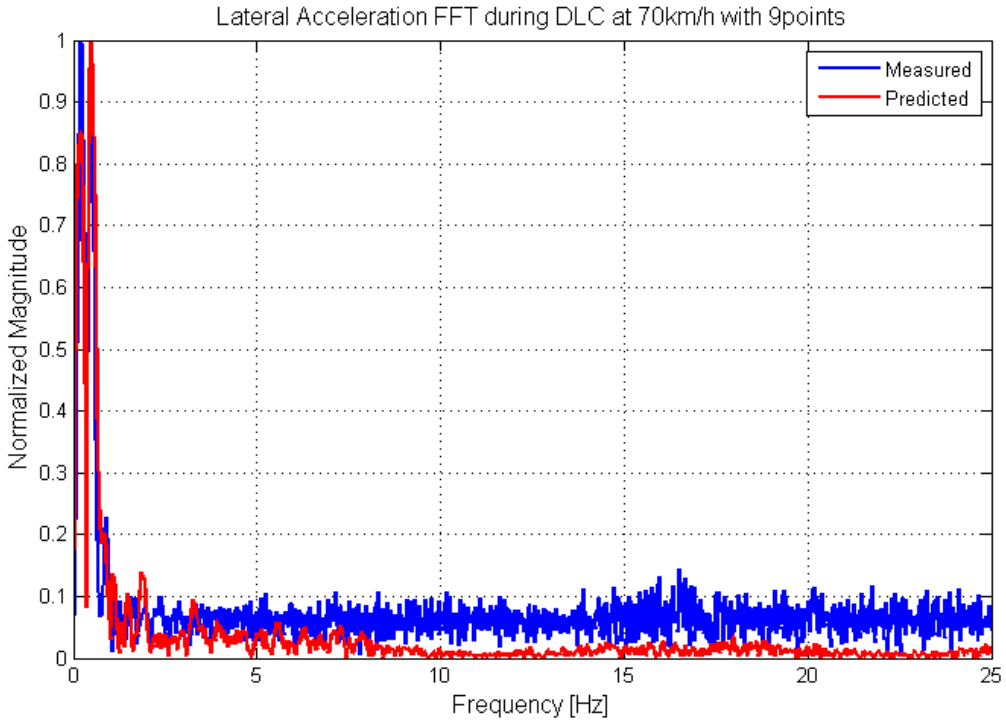

Figure 5-13: Lateral acceleration FFT during DLC at 70km/h with 9 points

Instead of adding noise to the predicted lateral acceleration, the measured and predicted lateral accelerations will be compared to one another and the biggest absolute acceleration of the two will be used as an output as written in Equation 5.6.

$$\begin{aligned} if\ |\ddot{y}_m| > |\ddot{y}_p|, \quad & \ddot{y}_{out} = \ddot{y}_m \\ if\ |\ddot{y}_m| < |\ddot{y}_p|, \quad & \ddot{y}_{out} = \ddot{y}_p \end{aligned} \tag{5.6}$$

Figure 5-14 shows the measured (blue), predicted (red) and output (green) lateral accelerations. The predicted lateral acceleration is not plotted with the preview time taken into account; this is done so the values at the current time step can be compared to one another.

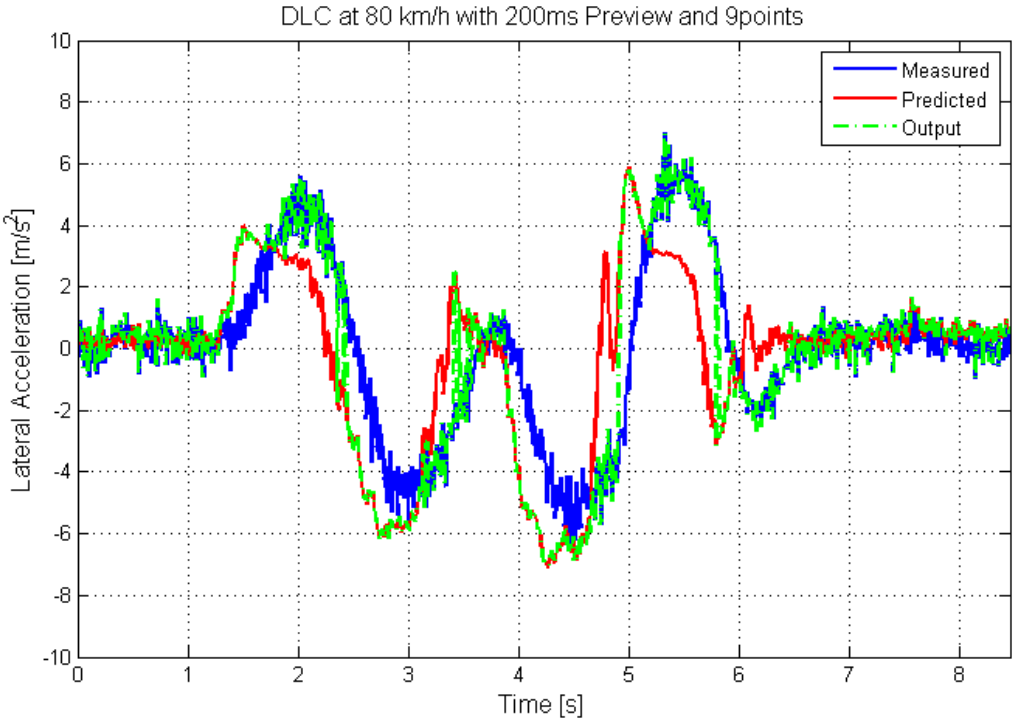

Figure 5-14: DLC at 80km/h with 200ms preview lateral acceleration output

It can be seen from Figure 5-14 that when the vehicle is driving in a straight line that the measured lateral acceleration becomes the output value and when the vehicle starts performing a manoeuvre, and the predicted lateral acceleration increases, the predicted lateral acceleration is used as an output. This method solves the problem of having predicted states that are less noisy than the measured states while simultaneously switching according to current and future conditions.

5.4 Speed Limits

Another part of the VPM that needs to be investigated is when the vehicle is stationary. In typical city driving conditions the vehicle encounters numerous stop-go situations due to traffic lights and stop streets.

The speed of the vehicle is measured using a VBOX, and according to the manufacturers it is able to measure a minimum speed of 0.1 km/h. This is indeed the case when the signal is logged on the internal memory of the VBOX, but when the speed is used as a real-time analog output from the VBOX to the VPM, it was found that a minimum speed of about 3 km/h is measured. This is due to noise from the surroundings and the fact that using the base station is not always possible when driving in the city.

Figure 5-15 shows the measured speed, some measured and predicted vehicle states and the suspension settings when the vehicle is stationary. It can be seen that, because the speed does not measure zero, the VPM predicts the vehicle states incorrectly and this causes spurious switching of the suspension.

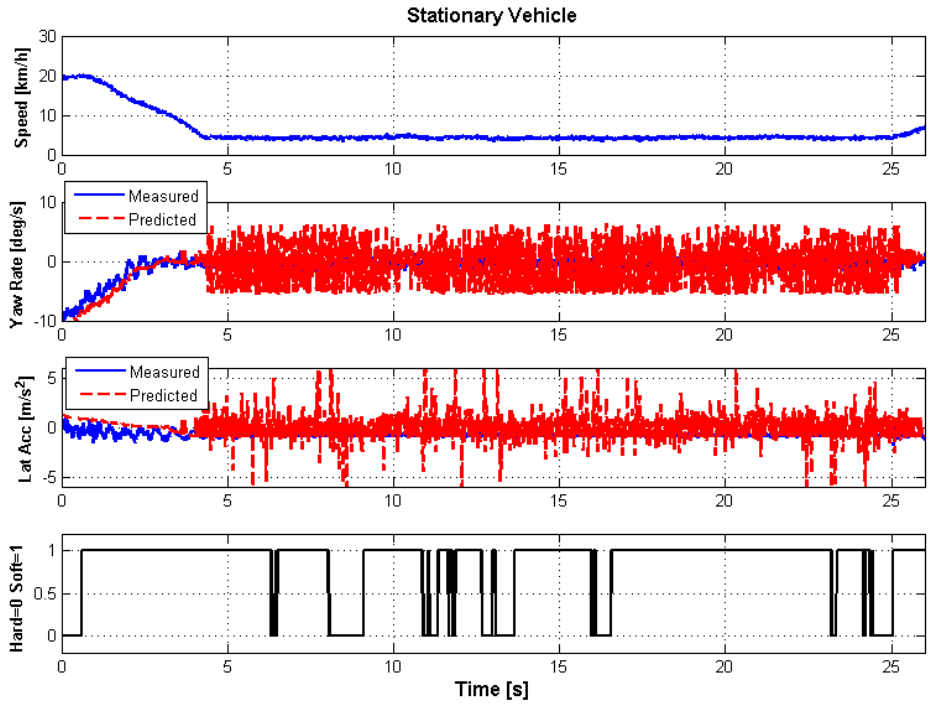

Figure 5-15: Stationary Vehicle Problem

This problem is easily solved by implementing a speed limit to the VPM. When the measured speed is lower than 10 km/h, the VPM will not be used and the measured lateral acceleration will be used directly as an output. In this case the predicted vehicle states that are saved will be made zero

and the results can be seen in Figure 5-16. It can also be programmed that at speeds below 10 km/h, the suspension setting might as well stay in ride comfort mode.

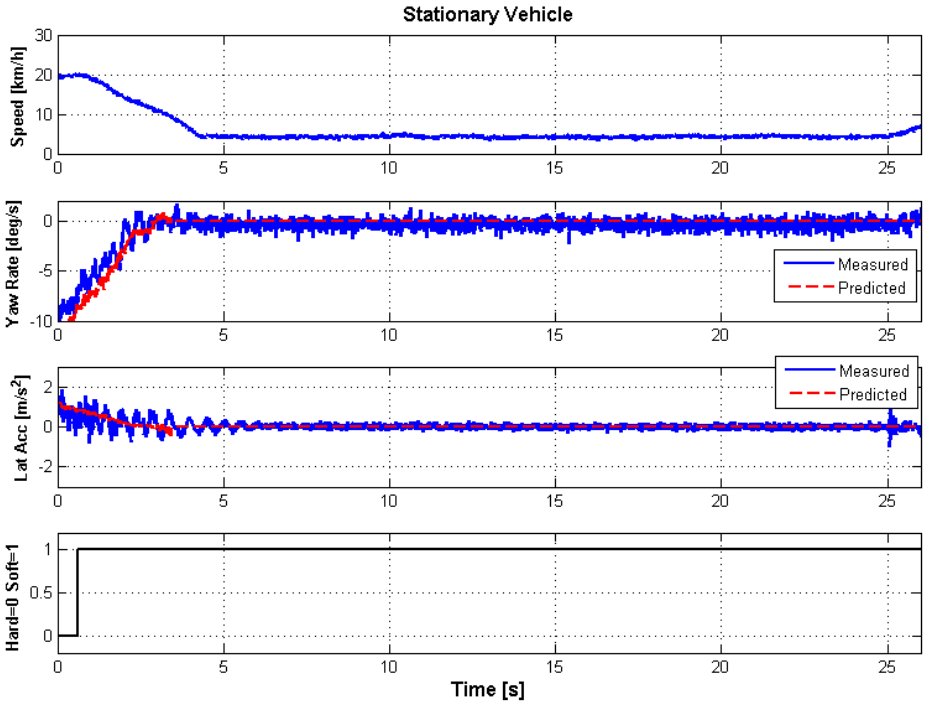

Figure 5-16: Stationary Vehicle Solution

5.5 Side-Slip Angle Measurement

At the moment, the side-slip angle of the vehicle is measured using a Correvit S-HR slip angle sensor that is mounted at the rear of the vehicle. The Correvit S-HR needs to be mounted roughly $250mm$ above the ground to obtain accurate side-slip angle readings. This piece of equipment is extremely expensive and damaging it cannot be afforded; it can only be mounted when performing tests in a controlled environment. For all city and highway driving, the model is run using a zero side-slip angle.

This means that the VPM makes a further assumption that the side-slip angle is negligible. To investigate the effect of this assumption on the accuracy of the VPM, DLCs are performed using the measured side-slip angle as well as a zero side-slip angle. The results are listed in Table 5-3 for the side-slip angle, yaw rate and lateral acceleration.

The side-slip angle predictions are more accurate when using the measured side-slip compared to assuming a zero side-slip angle. The effect on the yaw rate and lateral acceleration predictions is small, meaning that using the VPM with a zero side-slip angle still yields acceptable results.

If accurate side-slip angle information is required in a specific application, a less expensive way of measuring the side-slip angle or some kind of side-slip estimator needs to be implemented for the model to have an acceptable accuracy.

Table 5-3: R^2 with and without slip

Vehicle Parameter	R^2 with Side-Slip Angle	R^2 without Side-Slip Angle
Side-Slip Angle	0.92	0.66
Yaw Rate	0.90	0.91
Lateral Acceleration	0.93	0.91

Since a cheaper method of measuring the side-slip angle is not an option right now, a method of estimating the side-slip angle is suggested. This suggestion could be used to make the implementation of the VPM cheaper, or it could be used as a method of approximating different vehicle states.

Instead of measuring the side-slip angle of the vehicle, the VPM is used to estimate the side-slip angle and this side-slip angle will then be used by the VPM to predict the other vehicle states.

The preview time and exact method that needs to be used when estimating the side-slip angle needs further investigation before a thorough conclusion can be made. Simulation results show that using an estimated side-slip angle improves the accuracy of the predictions when compared to results obtained for no side-slip angle as seen in Table 5-4.

Table 5-4: R^2 comparing accuracy of model with different methods of obtaining the side-slip angle in simulation

Vehicle Parameter	R^2 with slip	R^2 without slip	R^2 with estimated slip
Side-Slip Angle	0.62	0.56	0.61
Yaw Rate	0.96	0.95	0.96
Lateral Acceleration	0.94	0.91	0.93

5.6 Conclusion

In this chapter the real-time performance of the VPM was investigated using the computing power available on the vehicle. The current VPM algorithm solves in real-time for preview times of up to 300 ms. The VPM performance and solving time can be improved significantly by changing the method by which the suspension forces are calculated or by using a more powerful computer.

The VPM was implemented to improve the RRMS switching strategy by decreasing the delay in the switching time. The switching delay was improved, but it wasn't a fair comparison as extremely noisy predictions were caused by noisy steer rate values. The steer rate was initially calculated using

the backwards differencing method of two consecutive steer angle values and this differentiation caused the noisy steer rate values. By using data points spaced 9 points apart, the noise in the steer rate values was reduced, yielding satisfactory prediction results.

The suspension also unnecessarily switched while the vehicle was stationary and a speed limit of 10 km/h was implemented to solve this problem. When the vehicle moves slower than the minimum specified speed, the measured lateral acceleration is used as input to the RRMS strategy instead of the predicted lateral acceleration preventing spurious switching of the suspension.

The Correvit S-HR which is used to measure the side-slip angle of the vehicle is an expensive piece of equipment and is mounted in such a way that it can be damaged when driving in the city. Therefore, the preview accuracy was investigated when making a further assumption that the side-slip angle is negligible and it was found that the VPM still yields satisfactory preview results for the lateral acceleration.

6 RESULTS

The results using the RRMS switching strategy combined with the VPM are shown in this chapter. This configuration is tested in a variety of ways. DLCs are performed to check that the suspension switches to handling mode earlier than the original RRMS strategy, which would improve the handling of the vehicle.

The vehicle is also driven around a Dynamic Handling track, designed to evaluate the handling characteristics of vehicle, using soft and hard suspension as well as the original RRMS strategy and the RRMS strategy combined with the VPM. This is done to check whether using the VPM improves the handling of the vehicle.

The strategy is also tested in typical city, urban and highway driving conditions to ensure that no spurious suspension switching occurs. These driving conditions mostly require the ride comfort suspension setting, except for short amounts of time when the vehicle negotiates a corner at higher speeds or when the vehicle is overtaking another vehicle.

6.1 Double Lane Change Tests

DLCs are performed on the Straight Track at the Gerotek Test Facilities (2013a) with different suspension settings as well as different speeds. Figure 6-1 shows the vehicle performing a DLC with the soft suspension setting, and the excessive body roll of the vehicle can be seen.

Figure 6-2 shows an extract of the results comparing the original RRMS and the RRMS combined with the VPM during a DLC performed at 80 km/h. The suspension switching for the original RRMS strategy is plotted with a solid blue line while the suspension switching for the RRMS strategy combine with the VPM with a preview time of 200 ms is plotted with a red dotted line. The RRMS strategy combined with the VPM switches 190 ms earlier than the original RRMS strategy.

The RMS values of the vehicle roll angle using different switching methods at different speeds are tabulated in Table 6-1 and shown in Figure 6-3. DLCs were performed at 50, 60, 70 and 80 km/h. It should be noted that 80 km/h is close to the maximum speed the vehicle can achieve through the DLC, meaning that the VPM is tested at the limits of the vehicle's capabilities. The original RRMS strategy is used, as well as the RRMS strategy combined with the VPM using preview times of 100, 200 and 300 ms. The original RRMS strategy is used as a benchmark to determine the improvement that the new strategy has on the handling of the vehicle.

When using the RRMS strategy combined with the VPM, it was found that the suspension switches from ride comfort mode to handling mode earlier than it did when only using the RRMS strategy. Since roll angle can be used to measure an off-road vehicle's handling ability (Uys et al.,

2006a), a significant improvement in the RMS value of the vehicle roll angle can be seen with an average improvement of 46% when using a VPM preview time of 300 ms.

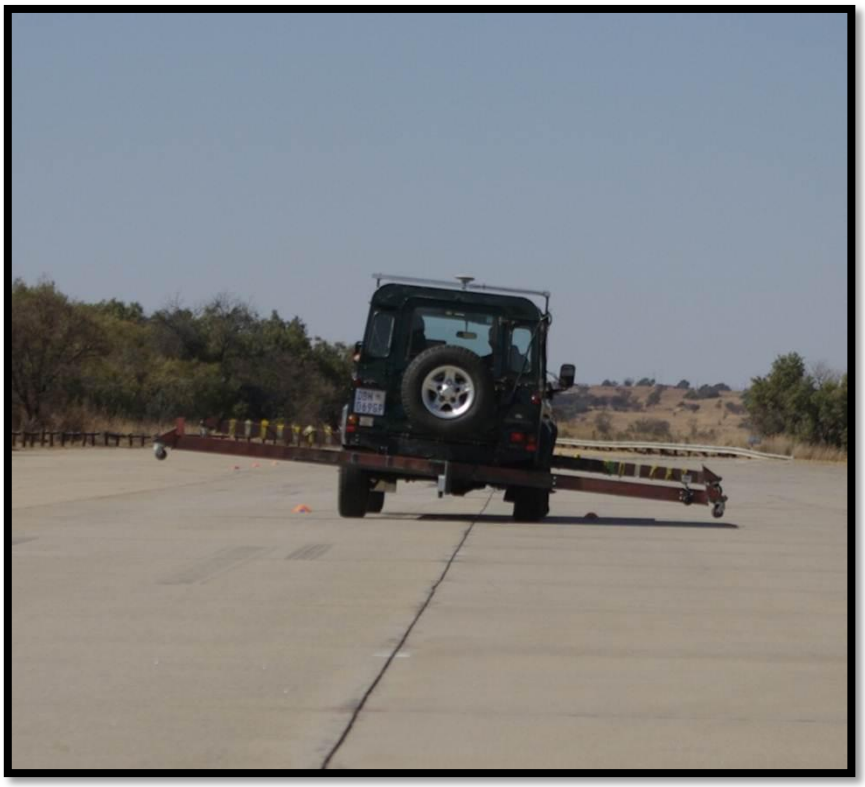

Figure 6-1: Vehicle during DLC

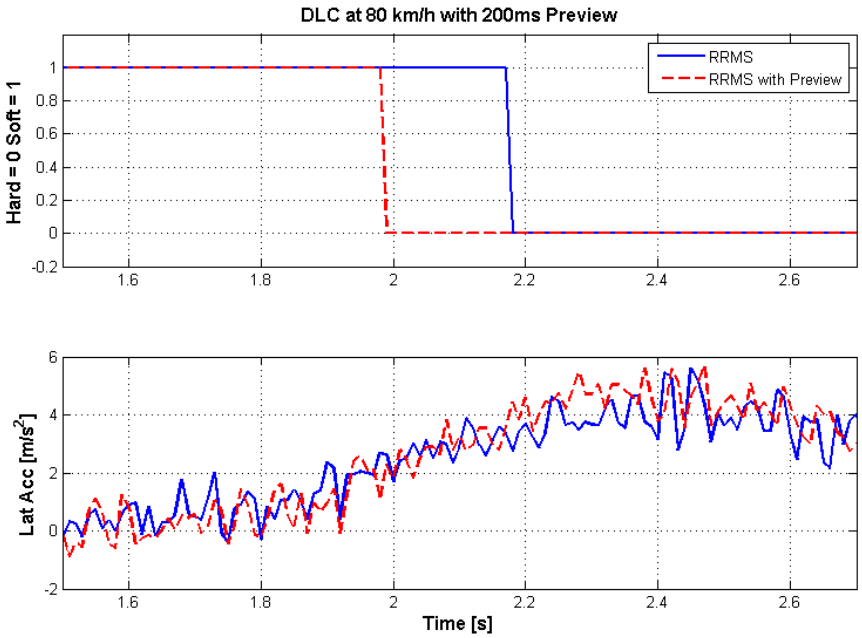

Figure 6-2: Suspension Settings Comparison

Table 6-1: RMS of the vehicle roll angle during DLCs

Double Lane Change			
Speed $[km/h]$	**Switching Method**	**RMS of Roll Angle**	**Percentage Improvement**
50	RRMS	1.203	
	RRMS with 100 ms Preview	0.997	**17%**
	RRMS with 200 ms Preview	0.792	**34%**
	RRMS with 300 ms Preview	0.535	**56%**
60	RRMS	0.965	
	RRMS with 100 ms Preview	0.822	**15%**
	RRMS with 200 ms Preview	0.702	**27%**
	RRMS with 300 ms Preview	0.601	**38%**
70	RRMS	1.191	
	RRMS with 100 ms Preview	0.83	**30%**
	RRMS with 200 ms Preview	0.928	**22%**
	RRMS with 300 ms Preview	0.622	**48%**
80	RRMS	1.146	
	RRMS with 100 ms Preview	1.102	**4%**
	RRMS with 200 ms Preview	0.888	**23%**
	RRMS with 300 ms Preview	0.668	**42%**

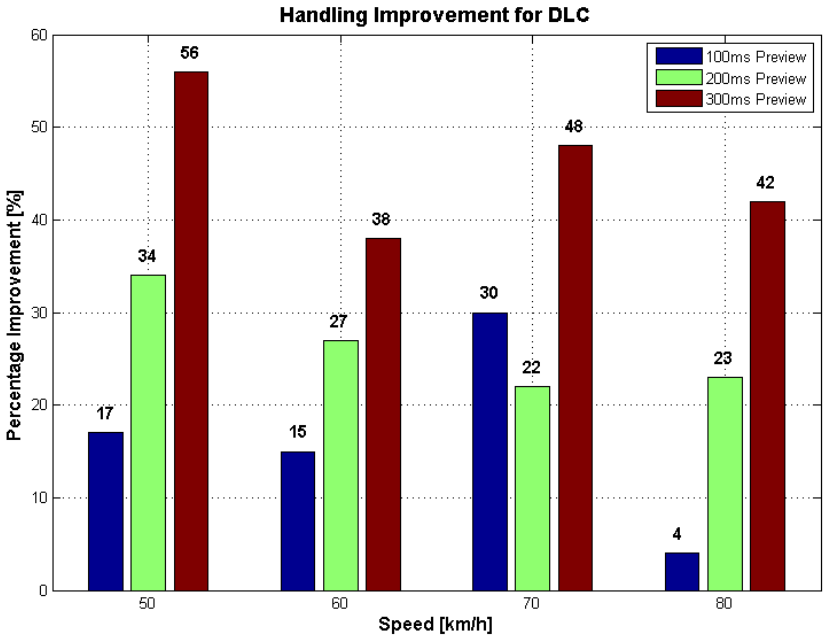

Figure 6-3: Handling improvement for DLC

6.2 Dynamic Handling Track Tests

The vehicle was driven around the Dynamic Handling track at the Gerotek Test Facilities (2013b) as shown in Figure 6-4. Laps were completed using soft and hard suspension settings, as well as the original RRMS strategy and the RRMS strategy combined with the VPM. The preview results using a preview time of 200 ms can be seen in Figure 6-5. An attempt was made to complete the different laps as consistently as possible by using the same driver and trying to complete the laps with similar lap times.

The laps were completed using the different strategies and the percentage time in handling mode and the RMS of the vehicle roll angle are tabulated in Table 6-2. It can be seen that the longer the preview time is, the more the vehicle is in handling mode, which improves the handling of the vehicle by decreasing the roll angle.

When using the RRMS strategy with a preview time of 300 ms, the vehicle is in handling mode for 68% of the lap compared to 65% for the original RRMS strategy. Even though the difference is only 3%, there is a 22% improvement in RMS value of the roll angle. The VPM lets the suspension switch a few hundred milliseconds earlier, which improves the handling of the vehicle. This makes it clear that, by reducing the switching delay, a significant improvement in vehicle handling is achieved.

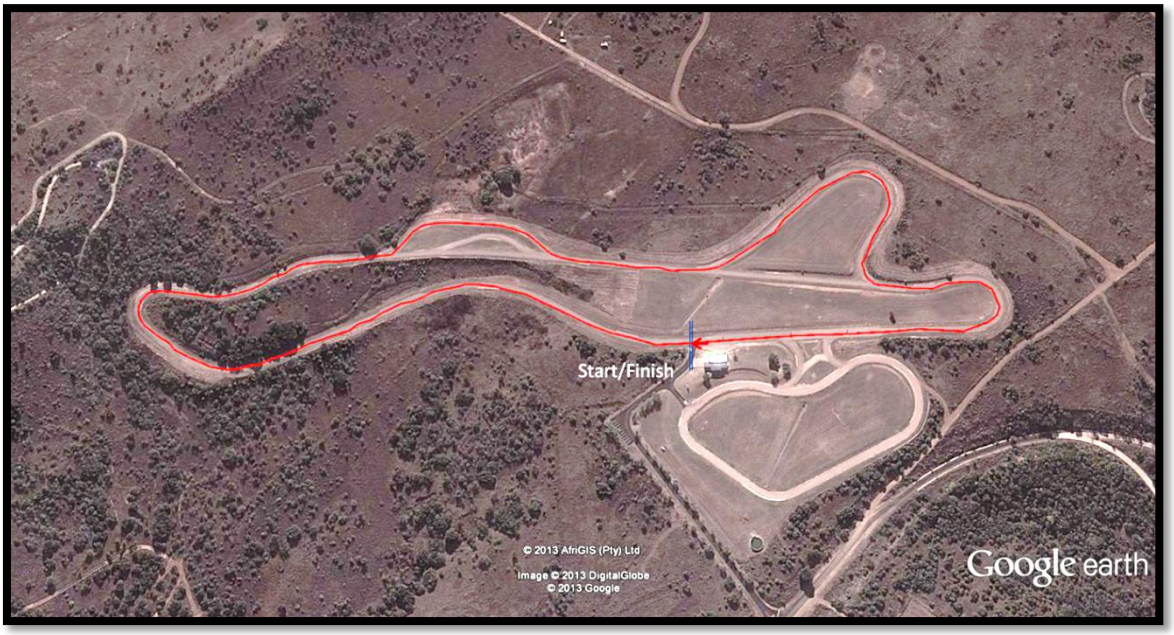

Figure 6-4: Dynamic Handling track at Gerotek (Google Earth, 2013a)

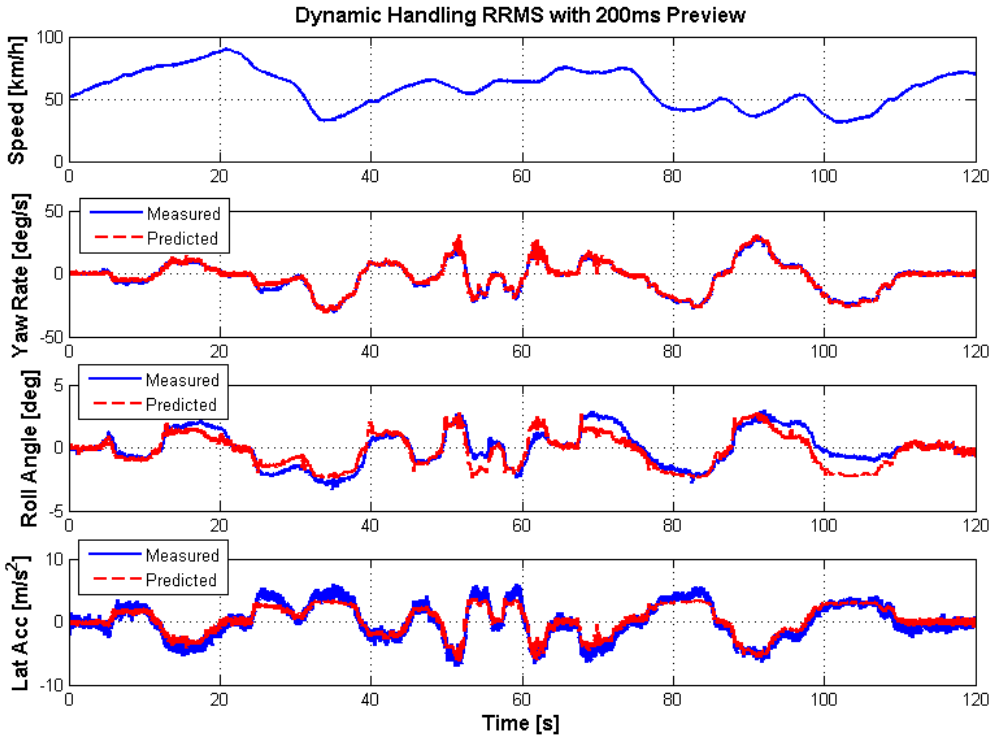

Figure 6-5: Dynamic Handling preview results with 200ms preview time

Table 6-2: Dynamic Handling Results

Strategy	Time in Handling [%]	RMS of roll angle	Percentage Improvement on RRMS
Soft	0	2.58	−47%
Hard	100	0.88	50%
RRMS	65	1.76	Baseline
RRMS with 200 ms	67	1.63	**7**%
RRMS with 300 ms	68	1.37	**22**%

6.3 City Driving Tests

The RRMS combined with the VPM strategy is thoroughly tested in typical city driving conditions, where more stop-start conditions are encountered due to traffic, stop streets and traffic lights. Figure 6-6 shows two extracts of the path the vehicle followed, part one is shown in red and part two is shown in blue. The preview results and suspension switching for part one and part two can be seen in Figure 6-7 and Figure 6-8, respectively.

Figure 6-6: City driving path (Google Earth, 2013b)

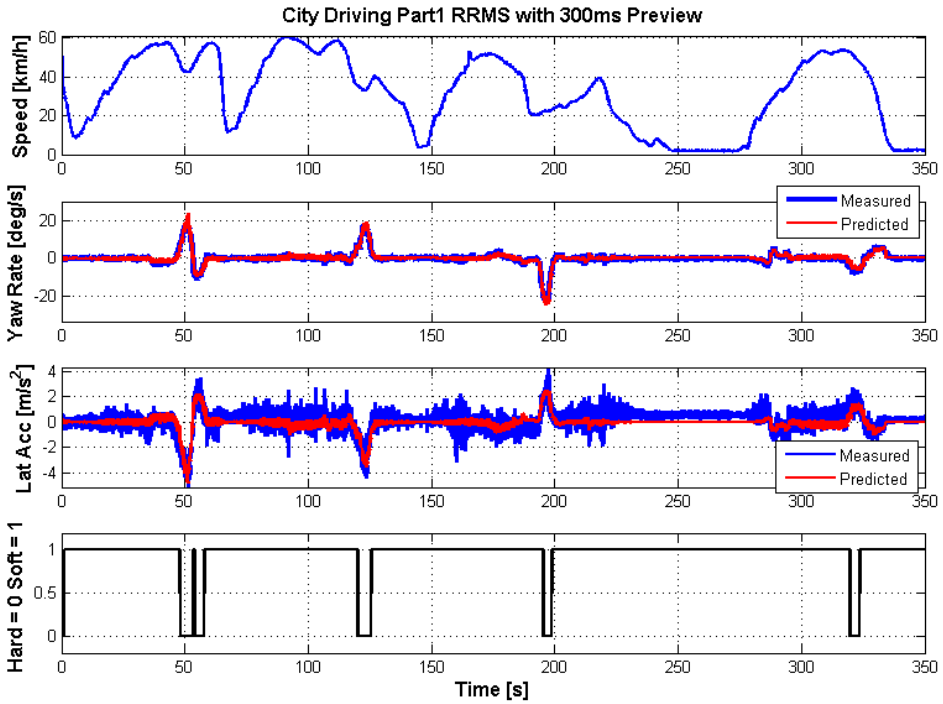

Figure 6-7: City driving part 1 using RRMS with 300ms preview

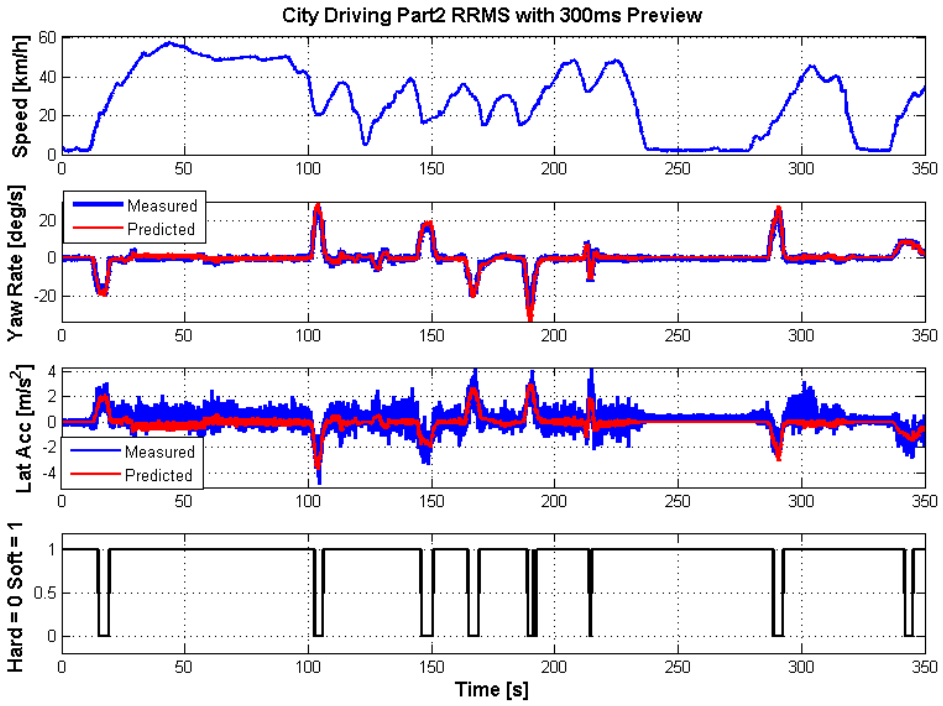

Figure 6-8: City driving part 2 using RRMS with 300 ms preview

After about 30 minutes of city driving with an average speed of 26.8 km/h and a maximum speed of 59.6 km/h, the suspension was in handling mode for 6.2% of the time, switching mostly while the vehicle negotiates corners. This seems high for a vehicle travelling at such low speeds.

It was also noted by the driver and the passenger that for certain corners the vehicle unnecessarily switched to handling mode. It is suggested that further a investigation should be done into some sort of speed limit, combined with the lateral acceleration limit implemented by Els (2006), that would prevent the vehicle from unnecessarily switching to handling mode.

6.4 Urban Driving

The new strategy was also tested on typical urban road conditions. This was done to ensure that the suspension does not switch unnecessarily. The path followed is shown in Figure 6-9 and an average speed of 57.6 km/h and a maximum speed of 93.3 km/h was achieved in this extract. The suspension was in handling mode for only 4.6% of the time. The predicted results and suspension switching are plotted in Figure 6-10, together with the measured results.

It can be seen that the RRMS strategy combined with the VPM successfully operates on urban roads. The vehicle only switched to handling mode when negotiating corners and no other spurious switching occurred.

Figure 6-9: Urban road path (Google Earth, 2013c)

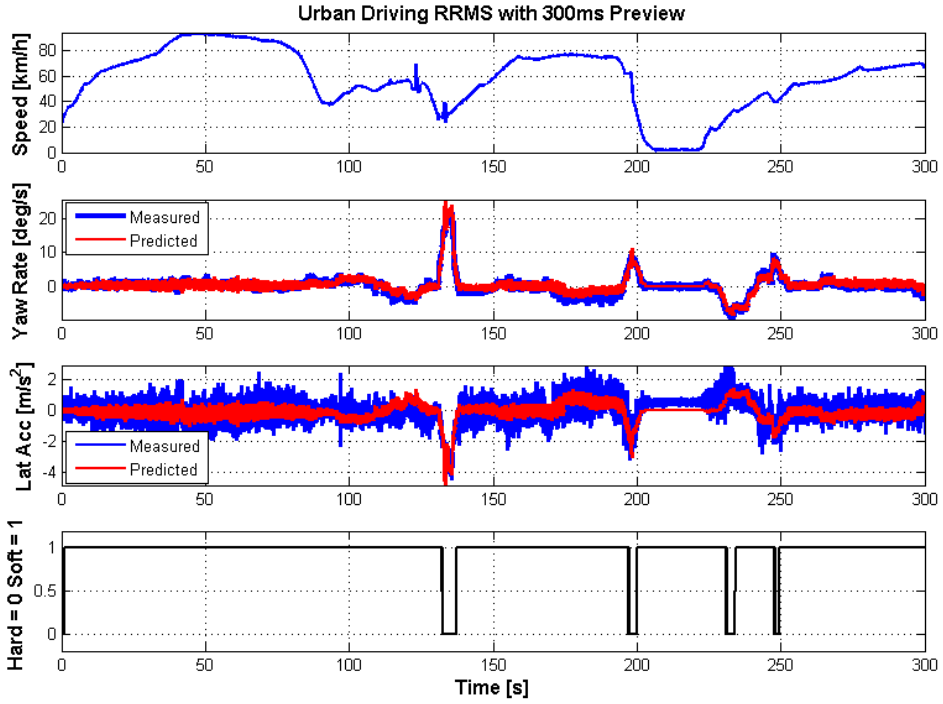

Figure 6-10: Urban driving using 300 ms preview

6.5 Highway Driving

Lastly, the new strategy was tested on the highway; Figure 6-11 shows the path that was followed. Figure 6-12 shows the measured and the predicted parameters as well as the suspension settings. It can be seen that the suspension only switched to handling mode for one part of the path being the

270° turn. After this the suspension did not switch again meaning that no spurious switching occurred.

Figure 6-11: Highway driving path 2 (Google Earth, 2013d)

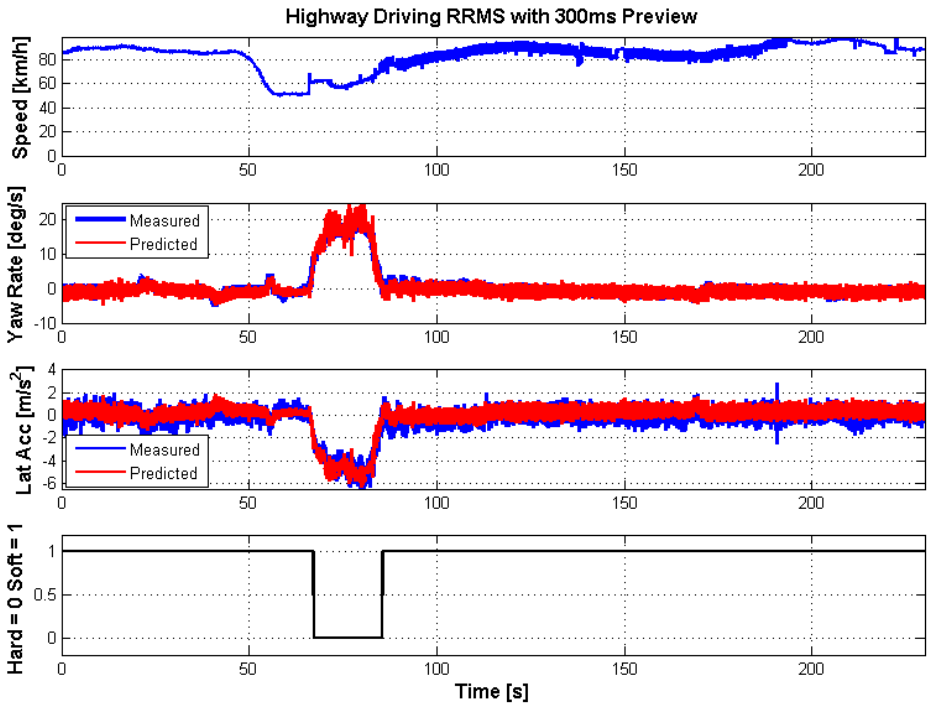

Figure 6-12: Highway driving Path 2 with 300 ms Preview

6.6 Conclusion

All these tests indicate that by using the predicted lateral acceleration of the VPM as an input to the RRMS strategy developed by Els (2006), that the handling of the vehicle can be improved. This new strategy was also tested in all types of conditions and yielded good results all round without any unnecessary suspension changes.

7 CONCLUSION AND RECOMMENDATIONS

7.1 Conclusions

Literature indicated that there are possible benefits to using some sort of preview. A VPM based on the Land Rover Defender 110 was developed and successfully validated against simulation and experimental data. The VPM accurately predicts vehicle states up to 390 ms, but only solves real-time up to 300 ms on the available processor.

The VPM was then implemented on the vehicle and further problems like noisy measurements and spurious suspension switching were resolved. Using the VPM in combination with the RRMS switching method yielded significant improvements in the roll angle and handling of the vehicle during DLCs and around the dynamic handling track. The new strategy achieved handling improvements of up to 56% compared to the original RRMS strategy.

It was also shown that no spurious switching occurs, making the RRMS strategy combined with the VPM an acceptable and stable method of switching the $4S_4$ between ride comfort and handling mode.

7.2 Recommendations

Improvements that can be made to the VPM will be discussed, as well as possible near future applications.

7.2.1 Suspension forces

Throughout the study, the inaccurate modelling of the suspension forces and suspension friction was mentioned. The friction in the suspension is known to have a major effect on the roll dynamics of the vehicle and causes the VPM to have inaccurate roll rate and, to a lesser extent, roll angle predictions. An investigation needs to be performed to better understand the exact suspension friction forces and how to model them accurately.

Another significant improvement that can be made to the VPM solving time, that is suspension related, is to use lookup tables for suspension forces instead of mathematical gas models. This would decrease the amount of calculation required. Els (2006) used an actuator to obtain the suspension characteristics of the $4S_4$ and these results can be used to generate a lookup table for faster suspension force estimators.

7.2.2 Real time CG estimation

The current VPM assumes that the CG of the vehicle remains fixed, which would be true if the vehicle is always used in the exact same setup as it was when the CG position was determined. It is known that loading a SUV, whether it be with passengers or luggage, changes the position of the CG, which has a major effect on the vehicle dynamics.

Having a good estimate of the CG position of the vehicle is extremely important to ensure accurate predictions. The current preview model uses the fixed CG position as determined by Uys et al. (2006b). Determining the CG position every time a passenger climbs in to or out of the vehicle is not viable, which means a different method of determining the CG position in real-time needs to used. Such algorithms have been developed in the past and should be implemented on the vehicle (Kolansky et al., 2013).

7.2.3 Tyre deflection

The roll angle of the vehicle is measured with lasers placed on the body. It means that the measured roll angle includes the vehicle body roll, relative to the axles, as well as the tyre deflection. Not being able to measure the exact tyre deflection, the model assumes that the tyre deflection has a negligible effect on the total roll angle. This is in fact not correct, as the tyres do deflect enough to have an effect on the roll angle. This problem can easily be solved by using the tyre stiffness and the vertical load at each tyre to estimate the tyre deflection.

7.2.4 Multiple VPMs

The test vehicle at the university has been equipped with different actuators and control systems to improve the handling of the vehicle. Only the $4S_4$ was used in this study, but other possibilities have also been used in the past, such as active anti-roll bars and rear wheel steering to improve the handling of the vehicle and to prevent rollover. The $4S_4$ struts were also switched in unison, but the vehicle is able to switch all four suspension struts independently of one another. By combining the methods listed below, a large number of vehicle configurations can be achieved.

- Each strut can individually be set to hard or soft spring and damper settings, giving the suspension on the vehicle 16 possible configurations.
- Changing the CG height of the vehicle by pumping oil in and out of the $4S_4$ struts.
- Variable anti-roll bar stiffness.
- Rear wheel steering.

These strategies have never been used at the same time, but rather each one on its own. If the characteristics of these methods can all be modelled, added to the VPM and solved in real-time, the

predicted states could be used as inputs to a control system that decides which combination of strategies would provide the best configuration to improve the current state of the vehicle.

By simultaneously solving a few VPMs (using different computers or multithreading), more information is available to make the required decision. To use the VPM in this way, the active anti-roll bar characteristics, the rate at which the vehicle is able to change the height of the CG, as well as the rear wheel steering need to be implemented in the VPM.

7.2.5 Side-Slip Angle Approximation

As discussed before, the instrument used to measure the side-slip angle on the vehicle is a piece of equipment that makes the implementation of the VPM expensive. The side-slip angle estimation capability of the VPM would make the implementation of the newly suggested strategy more viable.

REFERENCES:

Abe, M., 2009, Vehicle Handling Dynamics, Butterworth-Heinemann.

Blundell, M. and Harty, D., 2006, Multibody Systems Approach to Vehicle Dynamics, Butterworth-Heinemann.

Botha, T.R., 2011, High Speed Autonomous Off-Road Vehicle Steering, Unpublished Master's thesis, University of Pretoria, Pretoria, South Africa.

Cronje, P.H., Els, P.S., 2009, Improving off-road vehicle handling using an active anti-roll bar, J Terramechanics (2009), doi:10.1016/j.terra.2009.09.003.

Chen, B. and Peng, H., 2001, Differential-Braking-Based Rollover Prevention for Sport Utility Vehicles with Human-in-the-loop Evaluations, Vehicle System Dynamics, 36: 4, 359–389.

Diamond Systems, 2013, PC/104 SBC with Vortex86DX CPU and Integrated Autocalibrating Data Acquisition, Available at: http://www.diamondsystems.com/products/helios, Accessed 5 October, 2013.

Dukkipati, R.V., Pang, J., Quta, M.S., Sheng, G., Shuguang, Z., 2008, Road Vehicle Dynamics, SAE International, ISBN 978-0-7680-1643-7.

Els, P.S., 2006, The ride comfort vs. handling compromise for off-road vehicles, Unpublished PhD thesis, University of Pretoria, Pretoria, South Africa.

Gerotek Test Facilities, 2013a, Straight Track, Available at: http://www.armscordi.com/SubSites /Gerotek1/GEROTEK02_03_019.asp, Accessed, 5 October, 2013.

Gerotek Test Facilities, 2013b, Dynamic Handling Track, Available at: http://www.armscordi.com/SubSites /Gerotek1/GEROTEK02_03_08.asp, Accessed, 5 October, 2013.

Google Earth V 7.1.2.2041, 2013a, Gerotek Dynamic Handling Track, South Africa, 25°45'04" S 28°01'15" E, Accessed 5 October 2013.

Google Earth V 7.1.2.2041, 2013b, Pretoria City Area, South Africa, 25°45'23" S 28°13'30" E, Accessed 5 October 2013.

Google Earth V 7.1.2.2041, 2013c, Pretoria Urban Area, South Africa, 25°46'30" S 28°11'28" E, Accessed 5 October 2013.

Google Earth V 7.1.2.2041, 2013d, Pretoria Urban Area, South Africa, 25°45'04" S 28°16'26" E, Accessed 5 October 2013.

Governer's Office of Consumer Affairs, 2005, SUV rollover accident and death statistics, https://www.google.co.za/#q=Governer's+office+of+cosumer+affairs+SUV+rollover+accident+and+death+statistics, Accessed September 5, 2013.

International Organisation for Standardisation, ISO3888-1, 1999, Passenger cars, Test track for a severe lane-change manoeuvre – Part 1: Double lane-change.

Kolansky, J., Sandu, C., Botha, T.R. and Els, P.S., 2013, Real-Time Vehicle Parameters Estimation, Proceedings of the ASME IDETC/CIE 2013.

Pacejka, H.B., Bakker, E., Lidner, L., 1989, A New Tire Model with an Application in Vehicle Dynamics Studies, SAE paper 890087.

Road Traffic Management Corporation, 2009, Road Traffic Report for the Calendar Year 2009, http://www.arrivealive.co.za/documents/Year_2009_-_Road_Traffic_Report_-_V2.pdf, Accessed September 5, 2013.

Strashny A, 2007, U.S. Department of Transportation National Highway Traffic Safety Administration, An Analysis of Motor Vehicle Rollover Crashes and Injury Outcomes.

Thoresson, M.J., 2007, Efficient Gradient-Based Optimisation of Suspension Characteristics for an Off-Road Vehicle, Unpublished PhD thesis, University of Pretoria, Pretoria, South Africa.

Trent, V., Greene, M., 2002, A Genetic Algorithm Predictor for Vehicular Rollover 0-7803-7474-6/02/$17.00 ©2002, pp. 1752-1756.

Uys, P.E., Els, P.S., Thoresson, M., 2006a, Criteria for handling measurement, Journal of Terramechanics 43 (2006) 43-67.

Uys, P.E., Els, P.S., Thoresson, M.J., Voight, K.G., Combrinck, W.C., 2006b, Experimental Determination of Moments of Inertia for an Off-Road Vehicle with a Regular Engineering Laboratory, International Journal of Mechanical Education 34/4.

Van der Westhuizen, S.F., Els, P.S., 2012, Slow active suspension control for rollover prevention, J Terramechanics (2012), http://dx.doi.org/10/1016/j.jterra.2012.10.001.

Yim, S., 2011, Design of a Preview Controller for Vehicle Rollover Prevention, IEEE Transactions on Vehicular Technology, Vol. 60, No. 9, November, 2011.

Yi, K, Yoon, J., Kim, D., 2007, Model-based Estimation of Vehicle Roll State for Detection of Impending Vehicle Rollover, Proceedings of the 2007 American Control Conference, New York, USA.